TREND

Trapped Radiation Environment Model Development

Technical Note 6

Trapped Proton Anisotropy at Low Altitudes

ESTEC Contract No. 10725/94/NL/JG(SC)*

M. Kruglanski (IASB)

J. Lemaire (IASB)

April 1996

*ESA Technical Management: E.J. Daly (WMA)

Contents

List of Figures

List of Tables

Foreword

This Technical Note has been prepared in fullfilment of the Workpackage WP.2.2 of a project financed by ESA under the contract ESTEC No. 10725/94/NL/JG(SC). It describes two sets of models for the pitch-angle distribution and East-West asymmetry in the flux of energetic protons trapped into the geomagnetic field. It describes also the implementation of these models in the UNIRAD software package. The new software is called ANISO. It enables to predict from an omnidirectional flux model, like the AP-8 model, and a model for the atmospheric density scale heights, the flux of protons penetrating into a charged particle detector from any direction $\bar{D}$ with respect to the direction of magnetic field and azimuthal East-West direction.

Such a facility did not yet exist in the UNIRAD radiation environment software package nor in most other similar package used by other space agencies to calculate fluxes, fluences and radiation doses expected during future space missions in the Earth's magnetosphere. One of the alternative versions is based on the model originally developed at MSFC, while the other one is inspired by the proton pitch-angle distribution developed at JSC by Badwar & Konradi (1990). This software is now installed at the Belgian Institute for Space Aeronomy (BIRA-IASB) in Brussels and at ESTEC/WMA in Noordwijk.

Acknowledgments

We would like to thank Dr. E.J. Daly for his encouragement and support, as well as for his guidance during the development and realisation of this software and Technical Note. Hugh Evans also from ESTEC/WMA and Daniel Heynderickx from BIRA, must also be acknowledge for reading this Technical Note and for their useful comments and suggestions.

We wish also to thank the Director of the Belgian Institute for Space Aeronomy and his administrative and technical staff for their efficient support to the TREND-team activities.

Introduction

At low altitude, the high-energy trapped proton fluxes are strongly anisotropic and may induce anisotropies in the radiation exposure of a spacecraft with stabilized attitude. The flux anisotropy is understood theoretically by the interaction of the trapped protons with the Earth's atmosphere and by the finite length of the proton gyroradius. The main purpose of modelling this flux anisotropy is to deduce angular dependent proton flux spectra from standard omnidirectional flux data bases which were, until recently, the only ones available. Such a model has been developed analytically by Watts et al. (1989) and has been applied to evaluate radiation shielding for manned spacecraft (Armstrong et al., 1990; Appleby et al., 1992) and to analyse data from the LDEF satellite (Armstrong et al., 1992a and 1992b).

An anisotropy model is not included in the `UNIRAD` version 2.0. Within Work Package 2.2 of the TREND-3 study, the `ANISO` software modelling the trapped proton anisotropy effects has been developed at BIRA-IASB and implemented in `UNIRAD` version 2.1.

In Chapter 1 of this Technical Note, we review first the pitch-angle distributions of Heckman & Nakano (1969) and of Badhwar & Konradi (1990) and the East-West asymmetry as originally developed by Lenchek & Singer (1962). We investigate also the method to obtain the total anisotropy effect from the different angular distributions, as well as, the criteria that have to be met by the trapped proton anisotropy models.

In Chapter 2, we present the existing model of Armstrong et al. (1990) and a model based on Badhwar & Konradi (1990) distribution. The models are evaluated along a circular orbit for a fixed orientation of the satellite.

In Chapter 3, we describe the implementation of the `ANISO` software which provides the orbit-averaged unidirectional integral and differential fluences for a set of look directions.

Chapter 1

Description of the trapped proton anisotropy

At low altitude, the energetic proton flux is directly controlled by the density distribution of the Earth's atmosphere over a particle drift shell (Yoshida et al., 1960; Haerendel, 1962). The atmosphere induces two kinds of anisotropy in the directional flux of protons trapped in the Earth's magnetic field:

- the atmospheric loss cone causing a steep pitch-angle distribution,
- an East-West effect due to the finite size of the gyration radius.

The combined angular distributions give the total anisotropy of the directional proton flux. The model developed by Watts et al. (1989) takes into account the pitch-angle distribution proposed by Heckman and Nakano (1969) and the finite gyroradius effect described by Lencheck and Singer (1962).

After defining the notations used in the following paragraphs, the pitch-angle distribution models and the effect of the finite gyroradius length will be reviewed. Afterwards, their combination will be analysed and improvements will be proposed. Special attention will be drawn to the atmospheric scale height determination and to the Armstrong et al. (1990) models VF1MIN and VF1MAX. A trapped proton anisotropy model based on the Badhwar & Konradi (1990) pitch angle distribution will also be investigated.

1.1 Notations

In this section, we will introduce geometric planes and direction vectors defined at the location of observation. These planes and vectors and their relative orientation

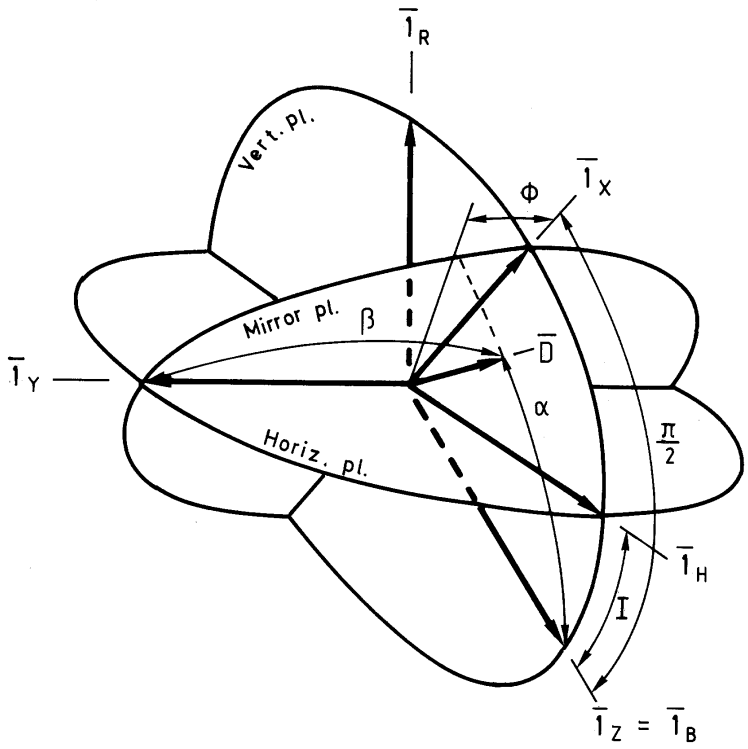

Figure 1.1. Representation of the coordinate system used in trapped proton anisotropy theory (see text)

are shown in Fig. 1.1. In this figure, the point of observation is located at the origin of the coordinate system. The local horizontal plane is represented, as well as the local vertical plane which contains the magnetic field line passing through the point of observation, and the plane perpendicular to the magnetic field line (mirror plane). The vector $\bar{D}$ represents an arbitrary direction which could be the look or viewing direction of a detector.

In a spherical geocentric coordinate system, the position of observation is characterized by the vector $R\,\bar{1}_R$ where R is the distance from the Earth's centre ($\bar{1}_R$ is the unit vector in the zenith direction). The altitude is given by $h = R - R_{\rm E}$, $R_{\rm E}$ being the Earth's radius. At this location, the geomagnetic field vector is denoted by $B\,\bar{1}_B$. In the northern hemisphere, the magnetic field vector points down to the Earth while in the southern hemisphere, it points upward away from the Earth.

A useful coordinate system is introduced with the z-axis along the magnetic field ($\bar{1}_z = \bar{1}_B$), the y-axis along the magnetic East direction ($\bar{1}_y \propto \bar{1}_B \times \bar{1}_R$) and the x-axis perpendicular to the magnetic vector in the vertical plane [$\bar{1}_x \propto (\bar{1}_B \times \bar{1}_R) \times \bar{1}_B$]. The magnetic dip angle I, i.e. the angle between the magnetic field and the horizontal

plane, is defined by $\cos I = \bar{1}_H \cdot \bar{1}_B$, where $\bar{1}_H = \bar{1}_R \times \bar{1}_y$ is the intersection of the horizontal plane and the vertical plane.

In a dipole magnetic field, the position of observation is also characterized by McIlwain's (1961) magnetic shell parameter L, the magnetic latitude λ and the magnetic longitude φ. The magnetic dip angle is related to λ by

$$2 \tan \lambda \;=\; \tan I \tag{1.1}$$

A vector $\bar{D}$ is specified in the coordinate system $(\bar{1}_x, \bar{1}_y, \bar{1}_z)$ by a polar angle α and an azimuthal angle ϕ. An angle β is also introduced which measures the deviation from the magnetic East direction ($\cos \beta = \bar{D} \cdot \bar{1}_y = \sin \alpha \sin \phi$).

The gyroradius of a charged particle with velocity parallel to $\bar{D}$, a charge q, a mass m_0 and kinetic energy E, is given by:

$$r_{\rm g} = \frac{r_{\rm gm}}{\sin \alpha} = \tilde{r}_{\rm g} \sin \alpha \tag{1.2}$$

(Hess 1968, Walt 1994), where $r_{\rm gm}$ is the gyroradius at the mirror point of the particle and where

$$\tilde{r}_{\rm g} = \frac{p}{qB} = \frac{\sqrt{E^2 + 2m_0c^2E}}{qcB} \tag{1.3}$$

is the gyroradius of a particle mirroring at the position of observation where the magnetic field intensity is equal to B; p is the relativistic momentum of the particle.

On the field line passing through the position of observation, the magnetic dip angle, the magnetic field intensity and the altitude of the mirror point are respectively $I_{\rm m}$, $B_{\rm m}$ and $h_{\rm m}$. For particles close to their mirror points at the position of observation*, it is convenient to introduce the deviation from a 90° pitch-angle: $\theta = \pi/2 - \alpha$.

Unidirectional flux

The unidirectional and differential flux of protons $j(E, \bar{D})$ of energy E is defined as the number of protons which hit per unit time a surface of unit area oriented perpendicularly to $\bar{D}$, and whose energy is in the interval E, $E + \delta E$ and velocity in the solid angle $\delta\Omega$. Therefore, the number δN of protons with energy between E and $E + \delta E$ and with a velocity vector in the solid angle $\delta\Omega$ in the direction $\bar{D}$, which hit the surface δA normal to the direction $\bar{1}_{\rm n}$, during a time interval δt, is given by

$$\delta N = j(E, \bar{D})\; (\bar{D} \cdot \bar{1}_{\rm n})\; \delta A\, \delta\Omega\, \delta E\, \delta t\,. \tag{1.4}$$

*When a particle is not close to its mirror point, it travels further along the field line down into the atmosphere and will be absorbed.

The integral unidirectional flux J is defined as

$$J(E,\bar{D}) = \int_E^\infty j(E',\bar{D})\,\mathrm{d}E' \,. \tag{1.5}$$

Without loosing generality the differential flux in the direction $\bar{D}$ can be expressed as

$$j(E,\bar{D}) = j_0(E)\ \left[\frac{1}{C}\,f(E,\theta)\,g(E,\theta,\phi)\right] \tag{1.6}$$

where $j_0(E)$ is the omnidirectional differential flux defined by

$$j_0(E) = \int_{4\pi} j(E,\bar{D})\,\mathrm{d}\Omega \tag{1.7}$$

and the second factor represents the angular dependence of the directional flux. The functions f and g are related respectively to the pitch-angle distribution and the azimuthal distribution with respect to the East-West direction. Note that f does not represent a phase-space distribution but represents a particle flux distribution; C is a normalisation factor.

1.2 Pitch-angle distribution

The pitch-angle distribution $f(\theta)\,\mathrm{d}\theta$ gives the flux of particles observed for pitch-angles between $\pi/2-\theta-\mathrm{d}\theta$ and $\pi/2-\theta$.

After the description of the origin of the pitch-angle anisotropy, the distributions of Heckman & Nakano (1969) and Badhwar & Konradi (1990) will be reviewed. These distributions will then be compared.

1.2.1 The origin of the pitch-angle anisotropy

The pitch-angle distribution is influenced by different processes depending to the drift shell. Through the conservation of the magnetic moment the pitch-angle distribution at any point of observation is related to the equatorial pitch-angle distribution $f_0(\theta)\,\mathrm{d}\theta$ on the same field line by

$$f(\theta) = \sqrt{\frac{B_0}{B}}\frac{\sin\theta}{\sin\theta_0} f_0(\theta_0) \tag{1.8}$$

where B_0 is the equatorial geomagnetic field intensity and $\theta_0 = \arccos(\sqrt{B_0/B}\cos\theta)$ the equatorial angle of deviation from 90°. Equation (1.8) clearly shows that the pitch-angle distribution could not be isotropic at every position along a field line.

At $L \geq 2$, the proton flux is controlled by radial diffusion (Schulz and Lanzerotti, 1974). On the outer edge, the population of the radiation belt protons is correlated to the injections associated with magnetic storms, and no particular pitch-angle anisotropy is expected. But, due to the radial diffusion and to the conservation of the first and second adiabatic invariants, a pitch-angle anisotropy appears and increases with decreasing L (Jentsch, 1984). Generally, the variation of the equatorial pitch-angle anisotropy is described with an anisotropy index N defined as†

$$f_0(\theta_0) = f_0(0)(\cos\theta_0)^N \tag{1.9}$$

where $f_0(0)$ reflects the equatorially mirroring proton flux (Garcia and Spjeldvik, 1985).

For θ close to the loss cone angle the energetic proton flux is directly controlled by the density distribution of the atmosphere over the particle drift shell (Yoshida et al., 1960) which enhances the anisotropy of the pitch-angle distribution $f(\theta)\,\mathrm{d}\theta$ and which is responsible for the loss cone. The main parameter controlling this pitch-angle distribution is h_m, the altitude of the mirror point. This altitude is related to θ through the formal relation

$$h_\mathrm{m} = h(B_\mathrm{m}) = h(\frac{B}{\cos^2\theta})\,. \tag{1.10}$$

In a realistic geomagnetic field, a particle reaches different altitudes at its mirror point locations, during its azimuthal drift path. Due to the eccentric displacement of the dipole moment of the geomagnetic field, the altitude variation is not negligible. As an illustration, we computed the geographical coordinates of mirror points corresponding to particles with different pitch-angles at a given point of observation. The altitudes h_m of the mirror points and their lowest values $h_{\widetilde{\mathrm{m}}}$ on the drift shell are given in Table 1.1, for different pitch-angles for a point of observation located at 90°E, 15°S and 2,000 km altitude in geocentric coordinates. The value h_m corresponds to the altitude of a mirror point located on the magnetic field line passing at the point of observation. The geographic location, the magnetic dip angle I_m and McIlwain's (1961) L_m of the mirror points are also listed. The values have been obtained using the Jensen and Cain (1962) geomagnetic field model.

For the protons passing through the point of observation, the minimum mirror point altitude $h_{\widetilde{\mathrm{m}}}$ decreases rapidly when the pitch-angle α steps away from 90°. This explains the loss cone and the sharp pancake like pitch-angle distribution peak around θ =0. When a mirror point is 600 km deeper inside the atmosphere, the corresponding atmospheric density increases by a factor of 2,000‡ and the corre-

†This pitch-angle distribution will not be used to describe the proton flux anisotropy at low altitude due to the absence of a loss cone in Eq. (1.9).

‡Using the Allen (1985) atmospheric model [Eq. (1.21)], $\rho(700\,\mathrm{km})/\rho(1300\,\mathrm{km}) \approx 25$, $\rho(500\,\mathrm{km})/\rho(1100\,\mathrm{km}) \approx 170$, $\rho(300\,\mathrm{km})/\rho(900\,\mathrm{km}) \approx 2300$, and $\rho(100\,\mathrm{km})/\rho(700\,\mathrm{km}) \approx 9 \times 10^5$.

Table 1.1. Geographical coordinates of mirror point (M.P.) for particles with different pitch-angle α at 90°E, 15°S and 2,000 km altitude. Jensen and Cain (1962) geomagnetic field model is used. $h_{\rm m}$ and $I_{\rm m}$ represent the altitude and the magnetic dip angle at the M.P.. In the right hand panel, the position of the deepest M.P. on the drift shell is given.

		M.P. along the field line				Drift shell lowest M.P.			
α	$L_{\rm m}$	$h_{\rm m}$	Lat.	Long.	$I_{\rm m}$	$h_{\tilde{\rm m}}$	Lat.	Long.	$I_{\tilde{\rm m}}$
90	1.55	2000.0	−15.00	90.00	46.6	827.8	−36.83	330.43	45.8
85	1.55	1989.0	−15.07	90.01	46.7	808.2	−36.95	330.55	45.9
75	1.55	1847.6	−15.96	90.12	48.1	649.9	−38.05	331.01	46.9
60	1.54	1378.0	−18.74	90.50	52.3	83.9	−40.70	335.44	50.5

Table 1.2. Geographical coordinates of mirror point (M.P.) for particles with different pitch-angle α at 90°E, 15°S and 2000 km altitude. GSFC 12/66 geomagnetic field model (Cain et al., 1967) , epoch 1970, is used. $h_{\rm m}$ and $I_{\rm m}$ represent the altitude and the magnetic dip angle at the M.P.. In the right hand panel, the position of the deepest M.P. on the drift shell is given.

		M.P. along the field line				Drift shell lowest M.P.			
α	$L_{\rm m}$	$h_{\rm m}$	Lat.	Long.	$I_{\rm m}$	$h_{\tilde{\rm m}}$	Lat.	Long.	$I_{\tilde{\rm m}}$
90	1.55	2000.0	−15.00	90.00	46.6	786.2	−34.71	333.06	47.2
85	1.55	1989.0	−15.07	90.01	46.7	767.1	−34.81	333.20	47.4
75	1.55	1848.0	−15.96	90.11	48.1	611.0	−35.89	333.59	48.5
60	1.54	1379.7	−18.73	90.48	52.3	58.9	−39.32	335.42	51.9

sponding particle flux dramatically decreases as well. In the right handside panel of Table 1.1 it is shown that when the particle passes through the South Atlantic Anomaly region, the mirror points penetrate deeply in the atmosphere, striking very high atmospheric densities. Therefore, the controlling parameter is the lowest mirror-point altitude $h_{\tilde{\rm m}}$ rather than the value of $h_{\rm m}$ which corresponds to the mirror point of the field line passing at the point of observation.

The values of $h_{\rm m}$ and $h_{\tilde{\rm m}}$ are given in Tables 1.2 and 1.3 for the same starting point as Table 1.1 but the field lines and drift shells are traced with two different geomagnetic field models. Table 1.2 corresponds to GSFC 12/66 (Cain et al., 1967) and Table 1.3 to IGRF 90. The comments are the same as for Table 1.1. However, while the altitudes corresponding to mirror points on the field line passing through

Table 1.3. Geographical coordinates of mirror point (M.P.) for particles with different pitch-angle α at 90°E, 15°S and 2000 km altitude. IGRF90 geomagnetic field model is used. $h_{\rm m}$ and $I_{\rm m}$ represent the altitude and the magnetic dip angle at the M.P.. In the right hand panel, the position of the deepest M.P. on the drift shell is given.

		M.P. along the field line				Drift shell lowest M.P.			
α	$L_{\rm m}$	$h_{\rm m}$	Lat.	Long.	$I_{\rm m}$	$h_{\widetilde{\rm m}}$	Lat.	Long.	$I_{\widetilde{\rm m}}$
90	1.54	2000.0	−15.00	90.00	46.1	679.6	−33.83	327.56	47.8
85	1.54	1989.0	−15.07	90.01	46.2	660.0	−33.97	327.62	48.0
75	1.53	1849.8	−15.96	90.13	47.7	501.3	−35.02	328.08	49.2
60	1.53	1386.9	−18.74	90.54	51.9	−62.3	−39.80	327.16	52.0

the point of observation (left panels) are nearly identical in all three cases, the altitudes corresponding to the lowest mirror points are quite different. These differences are due to the secular variation of the geomagnetic field[§] between 1960 and 1990.

According to their initial pitch-angles, the particles, passing through the point of observation, populate different drift shells (Roederer, 1970). The altitude variation of the lowest mirror point with the epoch—respectively 1960, 1970 and 1990 for Tables 1.1, 1.2 and 1.3—explains the artificial enhancement of the trapped radiation when an incorrect or inadequate geomagnetic field model is used to calculate B and L (Lemaire et al., 1990).

We now briefly describe the theoretical and empirical approaches which have been proposed to produce pitch-angle distribution models.

1.2.2 Heckman-Nakano pitch-angle distribution

The theoretical approach proposed by Heckman and Nakano (1969) assumes that the flux along a magnetic field line is inversely proportional to the atmospheric density at the mirror point location. This assumption is based on observations of the Explorer I satellite. In a large range of the Explorer I measurements, the radiation flux increases exponentially with the altitude (Yoshida et al., 1960). Considering as a first approximation that the atmospheric density varies as $\rho \propto \exp(-h/H)$, these observations support the assumption that the radiation flux is inversely proportional to the atmospheric density. This assumption was widely adopted [e.g. Haerendel (1962), Lenchek & Singer (1962)].

[§] The strength of magnetic Earth's dipole at Earth's surface decreases by 28.8 nT per year, and the dipolar offset increases by 2.5 km per year (Harwood and Malin, 1976; Fraser-Smith, 1987).

Heckman and Nakano (1969) expressed the angular distribution $f(\theta)\,\mathrm{d}\theta$ as the product of the probability P_1 that the particle has a pitch-angle between θ and $\theta + \mathrm{d}\theta$ and the probability P_2 that the particle is observed in a field line segment Δx. The probability P_1 is given by

$$P_1(\theta, \theta + \mathrm{d}\theta) \propto \frac{1}{\rho(h_\mathrm{m})}\,\mathrm{d}\ell\,, \tag{1.11}$$

where the pitch-angle range $[\theta, \theta + \mathrm{d}\theta]$ corresponds to a range $[\ell, \ell + \mathrm{d}\ell]$ of the mirror-point locations along the field line. The distance ℓ and the mirror-point altitude are approximatively related by $h_\mathrm{m} = h - \ell \sin I$.

The second probability P_2 takes into account the time $\Delta x / v_\parallel$ spent by the particle in the segment Δx (where $v_\parallel$ is the particle velocity along the field line) and τ_b the bounce period of the particle:

$$P_2 \propto \frac{\Delta x}{v_\parallel}\frac{1}{\tau_\mathrm{b}} \propto \sin^{-1}\theta\,. \tag{1.12}$$

Heckman and Nakano (1969) used a dipole field to obtain the relation between $\mathrm{d}\ell$ and $\mathrm{d}\theta$:

$$\mathrm{d}\ell = \frac{4}{3}R\left[\cos I(2 + \cos^2 I_\mathrm{m})\tan I_\mathrm{m}\right]^{-1}\tan\theta\,\mathrm{d}\theta\,. \tag{1.13}$$

In a small-angle approximation, $\tan\theta = \theta$, $\sin\theta = \theta$, $I = I_\mathrm{m}$, the integration of Eq. (1.13) gives

$$\ell = \frac{2}{3}R\left[(2 + \cos^2 I)\sin I\right]^{-1}\theta^2\,. \tag{1.14}$$

In an exponential atmosphere[¶], the pitch-angle distribution $f_\mathrm{HN}(\theta)\,\mathrm{d}\theta = P_1 P_2$ is given by

$$f_\mathrm{HN}(\theta)\,\mathrm{d}\theta \propto \frac{\mathrm{d}\theta}{\exp(-h_\mathrm{m}/H)} \propto \exp(\frac{-\theta^2}{2\sigma^2})\,\mathrm{d}\theta \tag{1.15}$$

where the square of the standard deviation is defined by

$$\sigma^2 = \frac{3}{4}\frac{H}{R}(2 + \cos^2 I) \tag{1.16}$$

and H is the atmospheric scale height. The Heckman-Nakano expression for the pitch-angle distribution has the advantage to be easy to use, but on the other hand, $f_\mathrm{HN}(\theta)$ is only valid for small values of θ, and it doesn't take into account the non-dipolar terms of the geomagnetic field.

Equation (1.16) shows that the Heckman-Nakano pitch-angle distribution does not depend on the atmospheric density but depends on the density gradient i.e.

[¶] An exponential atmosphere is given by $\rho(h) = \rho_0 \exp[-h/H]$ where H is the atmospheric scale height. Typically in an altitude range of 350–700 km, H varies between 50 and 100 km.

Table 1.4. Lowest mirror point altitude $h_{\widetilde{m}}$ of the drift shell (B_c, L_m) and the corresponding equatorial loss cone angle α_{L0} . B_c is the Vette's (1991) atmospheric cut-off magnetic field strength: $B_c = 0.6572B_0L^3.452$. The altitudes are given in km and the angles in degrees.

L_m	1.2	1.5	2.0	2.5	3.0
model \ α_{L0}	64.2	37.8	21.9	14.7	10.7
GSFC 12/66	213.4	185.0	81.1	−6.7	26.7
J. & C. 1962	234.4	202.4	150.5	82.9	79.7
IGRF 1990	145.0	56.9	−170.5	−333.3	−211.1

the density scale height. When the atmospheric scale height is small, the pitch-angle distribution becomes narrow when approaching θ =0. When the atmospheric scale height is larger, the pitch-angle distribution will spread and the small-angle approximation may no longer be valid. Note also that there is no true loss cone in the Heckman-Nakano formulation of the pitch-angle distribution.

1.2.3 Badhwar-Konradi pitch-angle distribution

Empirical pitch-angle distributions have been proposed (e.g. Valot & Engelmann 1973; Badhwar & Konradi 1990) and are characterised by the use of a loss cone angle α_L. The Badhwar-Konradi distribution is given by

$$f_{BK}(\theta) = \begin{cases} \xi \exp(-b\xi) & |\theta| < \pi/2 - \alpha_L \\ 0 & |\theta| > \pi/2 - \alpha_L \end{cases} \tag{1.17}$$

where $\xi = (\cos\theta - \sin\alpha_L)/\sqrt{B}$ and b is a shape parameter. The two parameters, α_L and b, have to be fitted to experimental unidirectional flux measurements. The Badhwar-Konradi distribution is an empirical fit function: it is not based on physical grounds: e.g. a pitch-angle diffusion theory. However, it gives an excellent fit for the AP-8 MIN omnidirectional fluxes, as well as for the measurements of Fischer et al. (1977).

When particles are inside the loss cone ($|\theta| > \pi/2 - \alpha_L$), they are precipitating into the atmosphere; these particles do not contribute to the flux intensity of trapped ions: there are no particles inside the loss cone. The parameter b controls the shape of the distribution defined by Eq. (1.17) for small values of θ.

The Badhwar-Konradi pitch-angle distribution does not depend explicitly on either the atmospheric density ρ or the atmospheric scale height H. This distribution

is connected to ρ and H through the loss cone $\alpha_{\rm L}$ and the empirical shape parameter b which have to be determined on a case by case basis to fit the experimental data sets.

Magnetic cut-off field intensity

The loss cone $\alpha_{\rm L}$ can be related to the atmospheric cut-off field intensity $B_{\rm c}$ which is the highest magnetic field intensity $B_{\rm m}$ for which the drift shell $(B_{\rm m}, L_{\rm m})$ is populated by stably trapped particles. $B_{\rm c}$ is a function of $L_{\rm m}$ and is directly related to $\alpha_{\rm L}$ by

$$\sin\alpha_{\rm L} = \sqrt{\frac{B_{\rm m}}{B_{\rm c}}}\,. \tag{1.18}$$

For the AE-8 model, an empirical formula for the magnetic cut-off field strength has been derived by Vette (1991) from the AZUR data. Vette's cut-off corresponds approximatively to a minimum altitude of 100 km along a drift shell. It is given by

$$\frac{B_{\rm c}}{B_0} = \begin{cases} 0.6572\, L_{\rm m}^{3.452} & \text{when } 1.2 \le L \le 3.23 \\ 1.0523\, L_{\rm m}^{3.050} & \text{when } 3.23 < L\,. \end{cases} \tag{1.19}$$

Since $L_{\rm m}$ is an adiabatic invariant in a static magnetic field distribution, B_0 and $B_{\rm c}$ are also adiabatic invariants where B_0 is the equatorial magnetic field intensity defined as: $B_0 = 0.311653/L_{\rm m}^3$ (Lemaire et al., 1990, 1995).

The equatorial loss cone is obtained from

$$\sin\alpha_{\rm L0} = (B_{\rm c}/B_0)^{-1/2}\,. \tag{1.20}$$

In Table 1.4, the lowest cut-off mirror point altitudes $h_{\rm m}^{\sim}$ for drift shells $(B_{\rm c}, L_{\rm m})$ are listed for different values of $L_{\rm m}$ and for three different geomagnetic field models. The first two geomagnetic field models (GSFC 12/66 and J.&C. 1962) are those used to build, respectively, the AP-8 MAX and AP-8 MIN model. The third row corresponds to the IGRF 90 geomagnetic field. The equatorial loss cone angle, $\alpha_{\rm L0}$, is also given.

It can be seen that the lowest mirror point altitude depends drastically on the geomagnetic field models used. These differences result from the secular variation of the geomagnetic field (see Footnote § on page 9). The best fit of Eq. (1.19) to a constant altitude line of mirror points is obtained with the Jensen and Cain (1962) geomagnetic field model, from which it had been determined.

The magnetic cut-off $B_{\rm c}$ or the loss cone angle $\alpha_{\rm L0}$ is different for different magnetic field and atmospheric models. The parameters $B_{\rm c}$ and $\alpha_{\rm L}$, and their dependence on $L_{\rm m}$ must be re-evaluated for each new dataset, and are specific to the epoch of the magnetic field model used.

1.2.4 Comparison between Heckman-Nakano and Badhwar-Konradi distributions

The Heckman-Nakano and the Badhwar-Konradi expressions correspond to two different approaches:

- Badhwar and Konradi (1990) propose an empirical fit function applied to an experimental trapped particle dataset (e.g. AP-8 MIN), while Heckman and Nakano's (1969) approach is a theoretical one which depends on a model of the atmospheric scale height and on an assumption linking the atmospheric density to the radiation flux.
- The parameter σ of the pitch-angle distribution $f_{\mathrm{HN}}(\theta)$ is defined locally in geographic coordinates, while the $f_{\mathrm{BK}}(\theta)$ parameters α_{L} and b only depend on E and L_{m}, as a consequence of Liouville's theorem (see Sect. 1.4.4).

The Badhwar-Konradi parameters α_{L} and b [Eq. (1.17)] have been obtained from a fitting procedure (Heynderickx and Lemaire, 1993) of an unidirectional version of the AP-8 MIN model where the value of L is determined using the Jensen and Cain (1962) geomagnetic field model and the energy is set to E =20 MeV (the parameters α_{L} and b vary slightly with energy).

To evaluate the Heckman-Nakano parameter σ [Eq. (1.16)], the atmospheric density scale height is obtained from functions fitted to an average atmosphere[‖] (Allen, 1985). The atmospheric number density or concentration in units of cm^{-3} can be approximated by

$$\rho(h) = \begin{cases} 10^{18.98} \exp\left(-\dfrac{h - 10\,\mathrm{km}}{6.5531\,\mathrm{km}}\right) & \text{when } 10\,\mathrm{km} \leq h \leq 120\,\mathrm{km} \\ 10^{11.69} \left(\dfrac{h}{120\,\mathrm{km}}\right)^{-7.0481} & \text{when } 120\,\mathrm{km} \leq h \leq 1,000\,\mathrm{km} \\ 10^{5.2} \left(\dfrac{h}{1000\,\mathrm{km}}\right)^{-2.7075} & \text{when } 1,000\,\mathrm{km} \leq h \end{cases} \tag{1.21}$$

(see Heynderickx et al. 1995) and the atmospheric scale height distribution can then be approximated by

$$H = -\frac{\rho(h)}{\mathrm{d}\rho/\,\mathrm{d}h} = \begin{cases} 6.5531\,\mathrm{km} & \text{when } 10\,\mathrm{km} \leq h \leq 120\,\mathrm{km} \\ h/7.0481 & \text{when } 120\,\mathrm{km} \leq h \leq 1,000\,\mathrm{km} \\ h/2.7075 & \text{when } 1,000\,\mathrm{km} \leq h\,. \end{cases} \tag{1.22}$$

[‖]For the purpose of this comparison, a simple atmospheric model is good enough. More realistic atmospheric model such as the semi-empirical model MSIS (Hedin, 1987 and 1991) may be used.

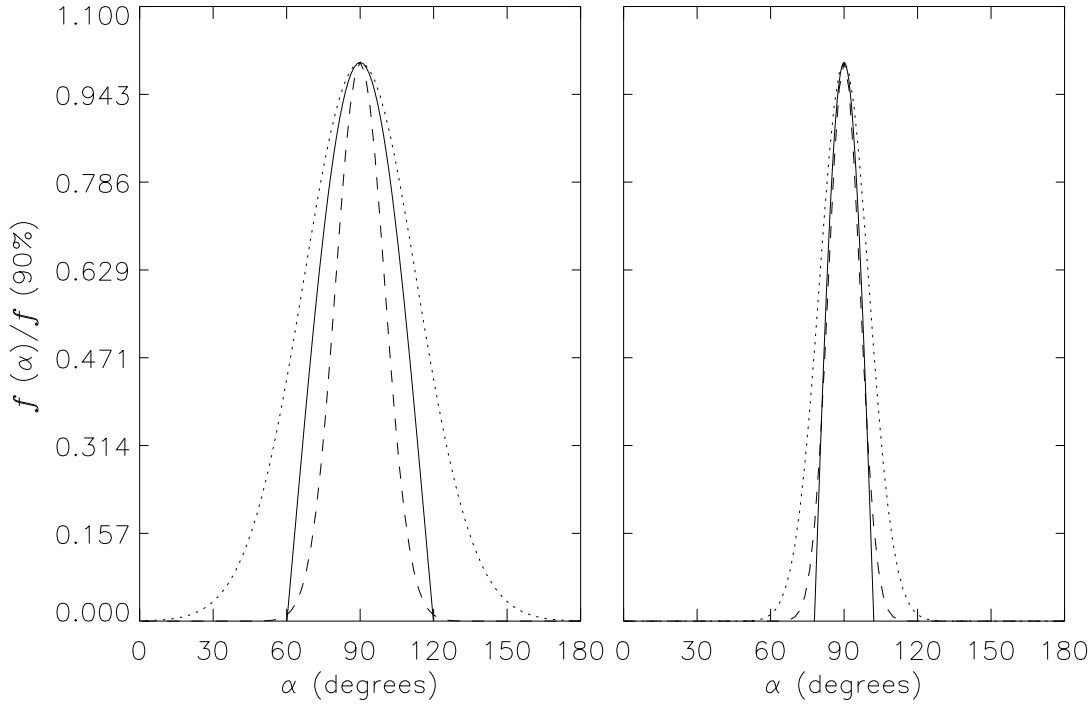

Figure 1.2. Comparison of the Heckman & Nakano (1969) and Badhwar & Konradi (1990) pitch-angle distributions for two different points of observation (altitude 2,000 km in the left panel and 700 km in the right one). The dotted and dashed lines represent respectively $f_{\rm HN}(\alpha)$ at the point of observation and at the lowest mirror point. The solid lines represent $f_{\rm BK}(\alpha)$.

In Fig. 1.2, the two approaches are compared at four different satellite positions coupled two by two: two coupled positions correspond to the locations of mirror points on the drift shell (L =1.55, $B_{\rm m}$ =0.1932), and the two other positions correspond to locations of mirror points on the drift shell (L =1.2, $B_{\rm m}$ =0.2158).

In the left panel of Fig. 1.2, the altitude of the point of observation is 2,000 km, the latitude is 15° and the longitude is 90°E as in Table 1.1; in the right panel the point of observation is located in the equator plane at an altitude of 700 km. For each of these points, we computed the (B, L) coordinates of the particles mirroring at the position of observation and we determined the position of the lowest mirror point on this drift shell. According to Badhwar and Konradi's (1990) approach, $f_{\rm BK}$ only depends on (B, L). As a consequence, the pitch-angle distribution $f_{\rm BK}$ (solid lines) is the same at both coupled points (i.e. at the initial mirror point and at the deepest mirror point). In the Heckman and Nakano's (1969) approach, $f_{\rm HN}$ depends on the local altitude, through σ and through the atmospheric scale height.

As a consequence, the different pitch-angle distributions are different at the point of observation (dotted lines) and at the lowest-altitude mirror point (dashed lines).

In the left panel, the point of observation is set to (2000 km, 15°S, 90°E) which corresponds to L =1.55, B =0.1932, $\alpha_{\rm L}$ =60.1°, $b = -0.9\,\mathrm{gauss}^{\frac{1}{2}}$ and σ =23.2°. As shown in Table 1.1, the deepest mirror point (dashed line) is located at 827.8 km, 36.8°S, 330.4°E where the value of σ is smaller: σ =9.9°.

The Badhwar-Konradi pitch-angle distribution (solid line) is steeper than the Heckman-Nakano distribution: beyond the local pitch-angle $\alpha_{\rm L}$, $f_{\rm BK}(\alpha)$ =0, whereas $f_{\rm HN}(\alpha)$ does not vanish within the loss cone. Remember, however, that for pitch-angles faraway from 90°, the Heckman and Nakano's small-angle approximation is no more valid. Compared to the Badhwar-Konradi pitch-angle distribution, the function $f_{\rm HN}$ is wider at high altitude (dotted line) and is smaller at low altitude (dashed line) for almost all pitch-angles. In that case, the function $f_{\rm HN}$ will produce a lower anisotropy at high altitude and a higher one at low altitude.

For all distributions, the unidirectional flux has been normalized to 1 at α =90°.

In that case, the pitch-angle distribution has to satisfy

$$\int_0^\pi f(\alpha)\sin\alpha\,\mathrm{d}\alpha = 1\,. \tag{1.23}$$

The omnidirectional flux can be used to renormalize these pitch-angle distributions.

According to Liouville's theorem (see Sect. 1.4.4) the pitch-angle distributions at the mirror point must be the same as at any mirror point on the same drift shell, including the lowest-altitude mirror point. As shown in the left panel, Expression (1.15) of Heckman and Nakano (1969) violates this rule. This is due to the fact that it does not take into account the averaged atmospheric scale height which is seen by the protons during their bounce oscillations and longitudinal drift.

In the right hand panel of Fig. 1.2, the point of observation is at 700 km, 0°N, 315°E which corresponds to $L = 1.2$, $B = 0.2158\,\mathrm{gauss}$, $\alpha_{\rm L} = 77.9°$, $b = -5.5\,\mathrm{gauss}^{\frac{1}{2}}$, $I_{\rm m} = 15.9°$ and $\sigma = 10.1°$. The second point is the lowest mirror point on the same drift shell. Its coordinates are (283.7 km, 26.2°S, 316.4°E) and $I_{\rm m} = 28.5°$ and $\sigma = 6.5°$. Since the altitude variations of the mirror points are smaller in the right panel than in the left panel, the drift shell averaged scale height is almost equal to the local values of the scale height. Therefore, both Heckman-Nakano pitch-angle distributions are closer to each other. Both $f_{\rm HN}$ distributions tend then to the Badhwar-Konradi function which fits correctly the fluxes of the unidirectional version of the AP-8 MIN model (Heynderickx & Lemaire 1993).

In conclusion, Heckman-Nakano's and Badhwar-Konradi's pitch-angle distributions produce qualitatively similar results. However, the Heckman and Nakano

(1969) results deviate from the expected result at higher altitude, i.e. when the mirror point is at a much lower altitude. The Badhwar and Konradi approximation is adiabatically invariant, since it depends only on the (B, L) coordinate system which are adiabatic invariants in a static magnetic field; this guarantees a satisfactory pitch-angle distribution at all altitudes. Since this empirical fit has been based on the AP-8 model, it would be useful to test whether f_{BK} fits also other directional proton flux observations.

1.3 Lenchek-Singer East-West asymmetry model

The Lenchek & Singer's model is the first and only one we know of, describing the azimuthal distribution of the trapped particle fluxes at low altitude where East-West effects become important.

As depicted by Lenchek and Singer (1962), for a given point of observation, protons coming from the West have their guiding centres above the point of observation, while those coming from the East have their guiding centres below this point. Therefore, during their drift, protons coming from the West will experience averaged atmospheric densities smaller than those with the same pitch angle but coming from the East. This East-West asymmetry is observable when the gyroradii of the trapped protons become comparable with the atmospheric scale heights, H.

For a proton at an altitude h with a velocity in the direction $\bar{D}$ (e.g. the axis of the detector), the altitude of the local guiding centre is given by $h + r_{\mathrm{g}} \cos I \cos \beta$. Let h_{m} be its mirror point altitude in the guiding centre approximation, i.e. on the field line passing through the point of observation. When the gyroradius is not small compared to the atmospheric scale height, its mirror point altitude will be given by $h_{\mathrm{m}} + r_{\mathrm{gm}} \cos I_{\mathrm{m}} \cos \beta_{\mathrm{m}}$. Assuming that the atmospheric density decreases exponentially with a scale height H and that the flux is inversely proportional to the atmospheric density at the mirror point (see discussion Sect. 1.2.2), the omnidirectional flux at h and h_{m} has to be corrected by a factor proportional to

$$\frac{\exp\left(-\dfrac{h_{\mathrm{m}}}{H}\right)}{\exp\left(-\dfrac{h_{\mathrm{m}} + r_{\mathrm{gm}} \cos I_{\mathrm{m}} \cos \beta_{\mathrm{m}}}{H}\right)} = \exp\left(\frac{r_{\mathrm{gm}} \cos I_{\mathrm{m}} \cos \beta_{\mathrm{m}}}{H}\right) . \tag{1.24}$$

Note that this correction depends on the local magnetic field configuration in the neighbourhood of the mirror point. Therefore, the correction factor may be different for all mirror points of a given drift shell $(B_{\mathrm{m}}, L_{\mathrm{m}})$.

In order to avoid field line tracing, the correction factor may be approximated

by

$$g_{\rm LS}(\theta,\phi) = \exp\left(\frac{\widetilde{r}_{\rm g}\cos I\sin\alpha\sin\phi}{H}\right) \tag{1.25}$$

when the pitch-angle is near 90°, $I_{\rm m} \simeq I$, $\beta_{\rm m} \simeq \beta$, $r_{\rm gm} \simeq \widetilde{r}_{\rm g}$, where $\widetilde{r}_{\rm g}$, the gyroradius of particles mirroring at the point of observation, is given by Eq. (1.3). The expression (1.25) has the advantage to be easy to use and to outline the dependence on the pitch-angle α and on the azimuthal direction ϕ.

Of course, when the gyroradius of a trapped ion becomes larger than the density scale height this first order approximation should become questionable. But so far no other alternative and more general theory has been proposed.

1.4 Combination of the angular distributions

In the previous sections, models for the pitch-angle and azimuthal distributions have been reviewed. In order to obtain the total angular distribution of the proton or heavier ion fluxes the pitch-angle distribution and the East-West asymmetry distribution must be combined and renormalized.

Let $f(E,\theta)$ be the pitch-angle distribution and $g(E,\theta,\phi)$ the distribution with respect to the East-West direction where $\theta = \pi/2 - \alpha$ is the complement of the pitch-angle, and ϕ is the azimuthal angle. The differential unidirectional flux then becomes

$$j = j_0(E)\,\frac{1}{C}\,f(E,\theta)\,g(E,\theta,\phi) \tag{1.26}$$

where j_0 is the omnidirectional trapped proton flux and C is a normalisation factor. Note that this decomposition of the unidirectional flux is not restrictive. The factor C and the functions f and g have to be determined so that the omnidirectional flux computed from Eq. (1.26) is equal to $j_0(E)$, i.e.

$$\int_0^{\pi}\int_0^{2\pi} j\ {\rm d}\phi\,{\rm d}\cos\alpha = j_0(E)\,. \tag{1.27}$$

There are different methods to satisfy this normalisation condition. Each method leads to a different expression of the unidirectional flux j, but each expression will provide the same omnidirectional flux j_0. Below, we restrict our description to the two most commonly used methods.

1.4.1 Global normalisation

The first method of normalisation is to define the factor C as

$$C = \int_0^{\pi}\int_0^{2\pi} f(E,\tfrac{\pi}{2}-\alpha)g(E,\tfrac{\pi}{2}-\alpha,\phi)\,{\rm d}\phi\,{\rm d}\cos\alpha\,. \tag{1.28}$$

In this case, the factor C is a constant, i.e. it depends neither on α nor on ϕ. For instance, when $g_{\rm LS}$ is used to describe the East-West asymmetry distribution, the integration over ϕ is analytical and the factor C is given by (Kern, 1989)

$$C_{\rm G} = 2\pi \int_0^{\pi} f(E, \tfrac{\pi}{2} - \alpha)\, {\rm I}_0\Big(\frac{\widetilde{r}_{\rm g} \cos I \sin\alpha}{H}\Big)\, {\rm dcos}\,\alpha \tag{1.29}$$

where $\rm I_0$ is the zero order modified Bessel function (Abramowitz and Stegun, 1964).

1.4.2 Separate normalisation

A second method of normalisation consists of normalizing separately the two functions f and g:

$$C_f = \int_0^{\pi} f(\tfrac{\pi}{2} - \alpha)\, {\rm dcos}\,\alpha \tag{1.30}$$

and

$$C_g = \int_0^{2\pi} g(\tfrac{\pi}{2} - \alpha, \phi)\, {\rm d}\phi\,. \tag{1.31}$$

In this case, the total normalisation factor is given by

$$C = C_f\, C_g\,. \tag{1.32}$$

Note that the total normalisation factor C now depends on the angle α. For instance, when $g_{\rm LS}$ is used to describe the East-West asymmetry, the factor C will be given by

$$C_{\rm S} = 2\pi\, {\rm I}_0\Big(\frac{\widetilde{r}_{\rm g} \cos I \sin\alpha}{H}\Big) \int_0^{\pi} f(\tfrac{\pi}{2} - \alpha)\, {\rm dcos}\,\alpha\,. \tag{1.33}$$

Obviously, the expressions (1.29) and (1.33) are different. These two expressions will lead to two different expressions for the unidirectional flux, but both will provide the same omnidirectional flux $j_0(E)$.

Therefore, a trapped proton anisotropy model is determined by a selection of an omnidirectional flux j_0, a pitch-angle distribution f, an azimuthal distribution g, and by the choice of the normalisation method: Eqs. (1.29) or (1.33).

1.4.3 Model of Watts et al. (1989)

Since the trapped proton anisotropy model proposed by Watts et al. (1989) is most largely used, we devote this section to its description.

The Watts et al. (1989) model for the total angular distribution of protons combines the Heckman and Nakano (1969) distribution with the Lenchek and Singer (1962) azimuthal distribution [Eq. (1.15) and (1.25)] where both distributions are normalized separately. Unlike the method depicted in Sect. 1.4.2:

– The Watts et al. normalisation of $f_{\rm HN}$ is obtained with respect to α instead of $\cos\alpha$; this leads to the approximate normalisation constant

$$C_{f\rm W} = \sin\alpha \quad \int_0^{\pi} f_{\rm HN}(\tfrac{\pi}{2} - \alpha)\,{\rm d}\alpha \tag{1.34}$$

where the $\sin\alpha$ has been put outside the integral. This may be justified by the assumption that at the lowest altitudes α is close to 90° and $\sin\alpha \simeq 1$.

– The normalisation of $g_{\rm LS}$ is performed numerically. The integral over ϕ (related to the Bessel modified function $\rm I_0$) is evaluated by the series expansion

$$C_{g\rm W} = 2\pi \sum_{k=0}^{\infty} \frac{1}{k!^2} \left(\frac{r_g \cos I \sin\alpha}{2H}\right)^{2k} \tag{1.35}$$

which converges rapidly (Evans and Daly, 1989).

A different result, probably more satisfactory, would be obtained with the normalisation factor C_S of Eq. (1.33).

Using (1.34) and (1.35), the Watts et al. (1989) directional flux distribution is then given by

$$j = j_0(E) \times \frac{\exp\left(-\dfrac{(\pi/2-\alpha)^2}{2\sigma^2}\right)}{\sin\alpha\sqrt{2\pi}\sigma{\rm erf}\left(\dfrac{\pi}{\sqrt{8}\sigma}\right)} \times \frac{\exp\left(\dfrac{r_g \cos I \sin\alpha \sin\phi}{H}\right)}{2\pi \displaystyle\sum_{k=0} \frac{1}{k!^2}\left(\frac{r_g \cos I \sin\alpha}{2H}\right)^{2k}} . \tag{1.36}$$

Due to the approximation made in Eq. (1.34), this unidirectional flux does not exactly reproduce the omnidirectional flux $j_0(E)$. However, the error remains very small except in the vicinity of α =0° and 180°, where Eq. (1.36) is singular. If a global normalisation would be used in the Watts et al. (1989) model, the normalisation factor would be given by Eq. (1.29). In this case C would not depend on α, and the unidirectional flux would be given by

$$j = j_0(E) \times C_{\rm G}^{-1} \exp\left(-\frac{(\pi/2-\alpha)^2}{2\sigma^2}\right) \exp\left(\frac{r_g \cos I \sin\alpha \sin\phi}{H}\right) . \tag{1.37}$$

Kern (1989) provides an approximate expression for the normalisation factor:

$$C_{\rm G}^{-1} \approx C_{\rm K} = \left(\frac{0.0750}{\sigma}\right)\left(0.8533 + \frac{r_g \cos I}{H}\right) \exp\left(-\frac{r_g \cos I}{H}\right) . \tag{1.38}$$

The factor C_{G} is well approximated by C_{K}^{-1} when $5^\circ < \sigma < 15^\circ$.

Both expressions (1.36) and (1.37) depend on the parameters h, H, B and I which are respectively the altitude, the atmospheric scale height, the magnetic field intensity and the magnetic dip angle. In the Watts et al. (1989) model, all these parameters are evaluated at the point of observation. Therefore, whatever the model used [Eq. (1.36) or (1.37)], the angular distribution of the proton flux varies from point to point on the same drift shell, which contradicts Liouville's theorem.

1.4.4 Liouville's theorem

As explained previously [see Eq. (1.26)], to create an anisotropy model, a pitch-angle distribution as well as a East-West asymmetry angular distribution must be selected or determined experimentally. Until a more comprehensive physical model is available, different criteria (e.g. the ease of use, the accuracy, etc.) will be used to select the appropriate distributions. In this section, we will study the constraint on the angular distribution functions f and g resulting from the application of the Liouville's theorem. This constraint affects the parameters on which the angular distributions depend.

In a stationary geomagnetic field and when magnetic field lines are electric equipotentials, the magnetic field intensity B_{m} at the mirror point and the McIlwain (1961) parameter L_{m} fully characterize a drift shell of trapped particles, i.e. the whole shell of guiding center field lines. Consider now unidirectional particle fluxes observed at two different locations $\bar{r}$ and $\bar{q}$ on a same drift shell. In the absence of Coulomb or wave-particle interactions, according to Liouville's theorem for trapped particles (Roederer, 1970; Hess, 1968), the fluxes are related by

$$\int_0^{2\pi} \frac{j(\bar{r}, \alpha_r, \phi_r)}{E}\, \mathrm{d}\phi_r = \int_0^{2\pi} \frac{j(\bar{q}, \alpha_q, \phi_q)}{E}\, \mathrm{d}\phi_q \tag{1.39}$$

In a stationary magnetic field, when the flux is assumed to be gyrotropic, the expression (1.39) reduces to $j(\bar{r}, \alpha_r) = j(\bar{q}, \alpha_q)$. The pitch-angles are determined by the conservation of the first adiabatic invariant i.e. the magnetic moment:

$$\frac{\sin^2 \alpha_r}{B(\bar{r})} = \frac{\sin^2 \alpha_q}{B(\bar{q})}\,. \tag{1.40}$$

At two points where the magnetic field intensities are equal, $\alpha_r = \alpha_q$ and

$$f(\bar{r}, \theta) \int_0^{2\pi} g(\bar{r}, \theta, \phi_r)\, \mathrm{d}\phi_r = f(\bar{q}, \theta) \int_0^{2\pi} g(\bar{q}, \theta, \phi_q)\, \mathrm{d}\phi_q\,. \tag{1.41}$$

This relation is the basic constraint on the angular flux distribution imposed by Liouville's theorem.

When the flux is gyrotropic (i.e. independent of ϕ), the constraint (1.41) shows that the pitch-angle distribution observed at conjugate points [i.e. with the same (B, L) coordinates] must be equal. This condition is satisfied by a pitch-angle distribution like f_{BK} given by Eq. (1.17), where the controlling parameters α_{L} and b depend on E and L_{m}. On the other hand, the pitch-angle distribution f_{HN} does not satisfied the condition (1.41), since the controlling parameters h, H and I of this pitch-angle distribution are evaluated at the point of observation. One way to meet the condition (1.41) with the Heckman-Nakano pitch-angle distribution would be to use effective parameters depending on coordinates such as B_{m} or L_{m} which both are adiabatic invariants in a static magnetic field. For instance, an effective scale height $H_{\rho'}$ may be defined as the scale height of the averaged atmospheric density over a drift shell (see Footnote ‡ ‡ on page 25).

When the azimuthal distribution due to the East-West effect is important, due to the constraint (1.41), the functions f and g are not independent from each other. A common practice is to simply meet separately the two following conditions:

$$f(\bar{r}, \theta) = f(\bar{q}, \theta) \tag{1.42}$$

and

$$\int_0^{2\pi} g(\bar{r}, \theta, \phi_r)\, \mathrm{d}\phi_r = \int_0^{2\pi} g(\bar{q}, \theta, \phi_q)\, \mathrm{d}\phi_q\,. \tag{1.43}$$

For instance, to satisfy the condition (1.43) with the Lenchek-Singer distribution [see Eq. (1.25)], one has to use an effective atmospheric scale height averaged over the whole drift shell. Furthermore, one has to use either a separate normalisation [see Sect. 1.4.2], or to restrict the application of the model to a simple centered dipole magnetic field.

In short, Liouville's theorem, which links particle flux observed at different locations on a drift shell, imposes a drastic condition [Eq. (1.41)] to the experimental or theoretical angular distribution for trapped proton directional flux models. When the separate normalisation [Eqs. (1.30) and (1.31)] is used, this criterion is reduced to Eq. (1.42). Therefore, parameters like (B_{m}, L_{m}, α_{L}, $H_{\rho'}$, $h_{\widetilde{\mathrm{m}}}$, ...) averaged over drift shells have to be preferred to local parameters like h, H, I to determine pitch angle distributions.

1.5 Atmospheric scale height

In the physical models for the angular distribution of trapped proton fluxes, the interaction of protons with the atmosphere is taken into account through parameters like the atmospheric density scale height H or the loss-cone angle α_{L} (see Sect. 1.2.2, 1.2.3 and 1.3). These parameters generally depend on the loss of energy and on the

rate of pitch-angle scattering of the particles along their drift trajectory. Therefore, to describe the trapped proton flux, an effective atmospheric scale height should be prefered to the local** scale height. In this section, we will focus on the method to calculate an effective atmospheric scale height from the trajectory of a particle and from its physical interaction with the atmospheric constituents.

The interaction of a particle with the atmosphere cannot be calculated over its detailed helicoidal trajectory due to limitations of computation time. Therefore some approximations or simplifications are required. In the sixties, most studies were focused on the evaluation of an effective atmospheric scale height averaged over a drift shell. For instance:

- Ray (1960) determined the expression of the averaged atmospheric density along a bounce path in a centred dipole magnetic field when the atmospheric density is decreasing exponentially. He calculated the scale height derived from these averaged densities and finally he related these scale heights to the spatial dependence of the proton flux.

- Blanchard and Hess (1964) used Ray's (1960) result to analyse the proton flux variation over a solar cycle.

- Newkirk and Walt (1964) traced drift shells in the guiding centre approximation. They studied the influence of the drift velocity or energy of the particles on the averaged (effective) atmospheric densities. They compared effective scale heights to the local scale height at the lowest mirror point of the drift shell. At L =1.25, they found that the effective scale height is about 10% greater than the local one at the lowest mirror point.

- Cornwall et al. (1965) calculated averaged atmospheric densities in the guiding center approximation for two different periods in the solar cycle. Below 200 km altitude, they found that the average atmospheric densities are independent of the phase in the solar cycle. However, as B_{m} decreases with altitude, the effects of the solar cycle become important.

- Hassitt (1965) extended the method of calculation and computed averaged atmospheric densities weighted by interaction cross sections. He deduced effective atmospheric scale heights for a large set of drift shells. He showed that latitude-independent atmospheric models were not able to reproduce Explorer-10 observed experimental flux at L =1.5.

**The local density scale height refers to the vertical profile of the atmospheric model at the point of observation, while the effective scale height is averaged over the drift shell.

– Heckman and Brady (1966) calculated effective atmospheric scale heights along helicoidal trajectories of the particles. At L =1.38, they found that the atmospheric density averaged over the trajectory of 125 MeV protons is about twice as large as the atmospheric density averaged over the trajectory of the guiding centers. They also discussed different ways to evaluate an approriate effective density scale height. At L =1.38, they showed that effective scale heights can be three to four times larger than the local scale height evaluated at the lowest mirror point.

The literature reviewed above contains different definitions of the average atmospheric density and of the density scale height. To determine the most approximate definition for the effective scale height one must first recall the physical processes of the interactions between protons with the atmospheric constituents.

To achieve a better understanding of the interaction of protons with the atmosphere let us recall the equation controlling the proton population in the inner zone of the radiation belts. On a given drift shell, the proton-population evolution is well described by the flux conservation equation (Freden and White, 1960)

$$\frac{\mathrm{d}N(E)}{\mathrm{d}t} = \mathcal{S}(E) - \mathcal{L}(E) - \frac{\mathrm{d}}{\mathrm{d}E}\left(N(E)\left\langle\frac{\mathrm{d}E}{\mathrm{d}t}\right\rangle\right) \tag{1.44}$$

where N is the number of protons with energy between E and $E + \mathrm{d}E$ in a unit volume element, $\mathcal{S}$ and $\mathcal{L}$ the source and loss terms. Equation (1.44) describes the time evolution of the proton energy spectrum trapped on this drift shell. The source includes cosmic-ray and solar-proton albedo neutron decay (Schulz and Lanzerotti, 1974). The loss term is due to nuclear collisions and charge exchanges with atmospheric constituents. It is given by

$$\mathcal{L} = vN(E)\sum_i(\sigma_i^{\mathrm{nc}}(E) + \sigma_i^{\mathrm{ce}}(E))n_i \tag{1.45}$$

where σ_i^{nc} and σ_i^{ce} represent respectively the nuclear-collision and charge-exchange proton cross section of the constituent i, v is the proton velocity and n_i the number density of the atmospheric constituent i. The charge-exchange mechanism is predominant for protons below 1 MeV (Liemohn, 1961). The nuclear interactions appear only for protons above 100 MeV. Therefore, the slowing down of protons due to the ionization and excitation of the atmospheric constituents [i.e. the last term of Eq. (1.44)] is the dominant process for proton energy between 1 and 100 MeV. The energy-loss rate is given by (Knoll, 1979):

$$-\frac{1}{v}\left\langle\frac{\mathrm{d}E}{\mathrm{d}t}\right\rangle = \frac{4\pi e^4}{m_0 v^2}\sum_i n_i Z_i \ln\left(\frac{2m_0 v^2}{\mathcal{I}_i}\right) \tag{1.46}$$

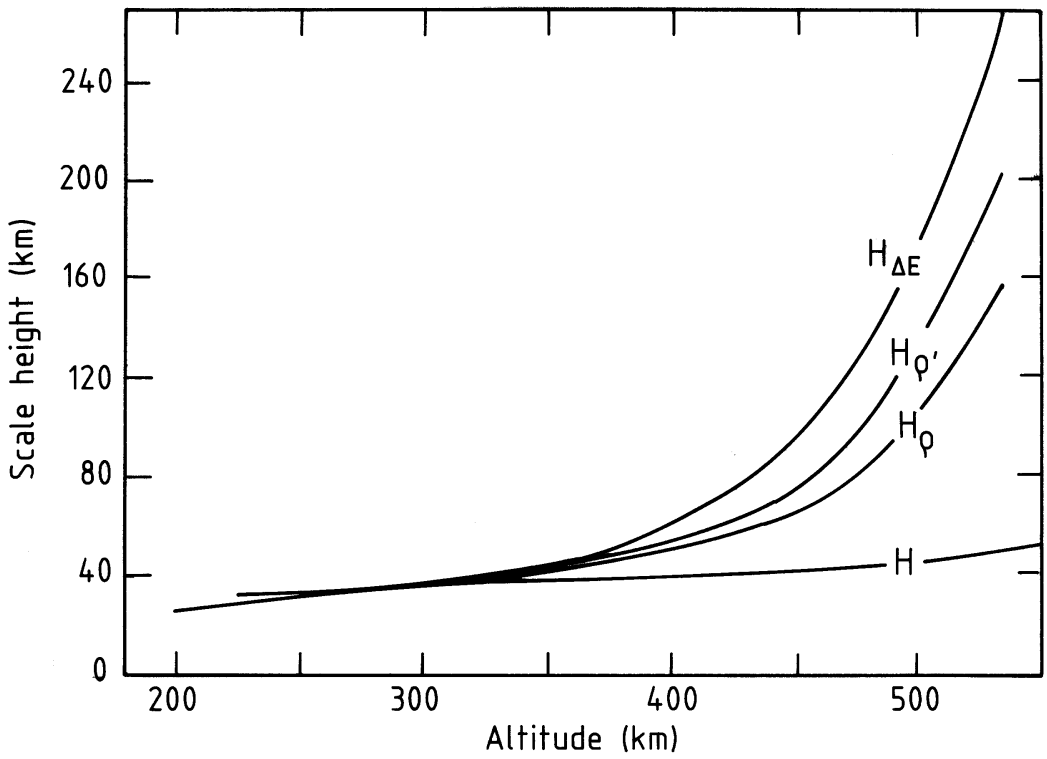

Figure 1.3. Atmospheric and effective scale heights versus altitude for 125 MeV protons at L =1.38. The atmospheric scale height is labeled H; H_ρ and $H_{\Delta E}$ are respectively the mass density and energy-loss scale heights averaged over the helicoidal particle trajectory; $H_{\rho'}$ is the mass density scale height averaged over the guiding-centre trajectory. (Heckman and Brady, 1966)

as a function of the ionization and excitation mean potential $\mathcal{I}_i$ of each constituent[††]; Z_i is the atomic number of constituent i; m_0 and e are respectively the electron rest mass and charge. The expression (1.46) represents an energy loss per unit length. Since the fractional energy loss per ionization collision is extremely small, this loss mechanism is described in Eq. (1.44) as a non-stochastic convective flow of $N(E)$ rather than a loss process.

In Eqs. (1.45) and (1.46), the atmospheric interaction determined by the number density n_i of the atmospheric constituents and not by the atmospheric mass density. The atmospheric mass density is given by

$$\rho = \sum_i m_i n_i \tag{1.47}$$

[††]The values of $\mathcal{I}_i$ for neutral constituents H, He, N, O are respectively 15, 42, 88 and 101 eV (Fano, 1963). For collisions with free electrons the logarithmic term in Eq. (1.46) becomes $\ln\left(\frac{\lambda_D m_0 v}{\hbar}\right)$ where λ_D is the plasmaspheric Debye length.

where m_i is the atomic mass of the constituent i.

On the other hand, in phenomenological approaches, the interaction of protons with the atmosphere is described in terms of global parameters such as averaged atmospheric densities and averaged scale heights. In this kind of approach (see Sect. 1.2.2 and 1.3), the interaction is related to the atmospheric density scale height H by an expression like

$$\frac{\mathrm{d}\ln j}{\mathrm{d}r} \approx \frac{1}{H} \tag{1.48}$$

where r is the radial distance along a field line.

To better take into account the interaction processes of the protons with the atmosphere in Eq. (1.48), the atmospheric scale height is usually replaced by an effective one. For instance, this effective scale height may be deduced from atmospheric densities which are weighted by interaction cross section and averaged over a drift shell.

Since in a wide energy range (1–150 MeV) the slowing down of protons are mainly due to ionization and excitation processes, the effective scale height should be deduced from the energy loss experienced by a particle along its trajectory:

$$\Delta E = \int \frac{1}{v} \left\langle \frac{\mathrm{d}E}{\mathrm{d}t} \right\rangle \mathrm{d}s \tag{1.49}$$

where the integral extends over the whole helicoidal trajectory of the particle during its drift motion. The energy loss rate is given by Eq. (1.46).

In Fig. 1.3, a local atmospheric scale height $H = -(\mathrm{d}\ln\rho/\mathrm{d}h)^{-1}$ and different effective scale heights evaluated by Heckman and Brady (1966) for L =1.38 are presented. They used the Jensen and Cain (1962) geomagnetic field model and Johnson's (1965) atmosphere for solar-minimum condition. The ionization energies $\mathcal{I}_i$ are obtained from Barkas and Berger (1964). The different effective scale heights shown in Fig. 1.3 are evaluated[‡‡] from

- the total amount of atmospheric mass traversed by a proton during its helicoidal trajectory (H_ρ);
- the total amount of energy lost by a proton during its helicoidal trajectory ($H_{\Delta E}$);

[‡‡] The effective scale height relative to the quantity φ is calculated as

$$H_\varphi = -\left(\frac{\mathrm{d}\ln\varphi}{\mathrm{d}h_{\tilde{\mathrm{m}}}}\right)^{-1} \tag{1.50}$$

where $\mathrm{d}h_{\tilde{\mathrm{m}}}$ is the variation of the lowest mirror-point guiding-centre altitude.

– the total amount of atmospheric mass traversed by a proton during its helicoidal trajectory when the atmospheric density is set equal to the density at the particle guiding centre ($H_{\rho'}$).

In Fig. 1.3, the effective scale heights H_ρ, $H_{\Delta E}$ and $H_{\rho'}$ are presented for 125 MeV protons at L =1.38 as a function of the lowest mirror point altitude $h_{\widetilde{m}}$. They are compared to the local atmospheric scale height H which is a slowly increasing function of the altitude.

Below 300 km, $H_{\Delta E}$ is equal to H_ρ. The main atmospheric constituents are N_2, O_2 and O which have similar ionization potentials and similar ratios A_i/Z_i (A_i is the atomic mass number of constituent i). The rate of energy loss [Eq. (1.46)] therefore becomes proportional to the atmospheric density.

Above 300 km, $H_{\Delta E}$ is greater than H_ρ for 125 MeV protons. At higher altitude, the relative number densities of He and H increase with height due to molecular diffusion of these atoms in the thermosphere. Since these atoms have different mass to charge ratios A_i/Z_i than N_2, O_2 and O. The energy loss rate of Eq. (1.46) is then no longer proportional to the atmospheric density and both effective scale heights differ from each other.

It can be seen from Fig. 1.3 that $H_{\rho'}$ differs also from H_ρ. A particle always penetrates into a denser part of the atmosphere below its guiding centre and in a less dense part above its guiding centre. However, on the average, the net result is that a particle experiences lower effective scale height along its helicoidal trajectory than at its guiding centre.

Above 400 km, the effective scale heights of each atomic constituent increase much faster with altitude than the local atmospheric scale height at the lowest mirror point.

In conclusion, the procedure to evaluate an effective scale height in a given atmospheric model has to be carefully reexamined. The scale height at the lowest mirror point of the drift shell is not always the appropriate one: it has to be evaluated over the whole drift shell. Ideally, the helicoidal trajectory of the particle should be used (instead of the trajectory of the guiding center). Moreover, the interaction of the particle with other species depends on different processes according to the energy of the particle and to the charge of the species. It would be useful to develop a new trapped proton anisotropy model based on the above-mentioned considerations. The angular flux distribution in this new model should, of course, satisfy the constraint resulting from Liouville's theorem and should depend on the energy loss by a particle along its drift shell rather than on a local or averaged atmospheric density. These specifications could be met by the use of a separate normalisation and a theory for the angular distribution similar to the theories of Heckman & Nakano (1969) and Lenchek & Singer (1962), but adapted to a scale height $H_{\Delta E}$ based on ΔE rather

than on the atmospheric density.

Chapter 2

Trapped proton anisotropy models

When a satellite has a high spin rate, its exposure to corpuscular radiation is generally calculated as if the proton flux would be isotropic. But, for instance, when the spin axis is aligned along the geomagnetic East/West direction, the radiation exposure can no more be assumed as isotropic due to the significant East-West effect at low altitude.

A trapped proton anisotropy model is intended to predict the unidirectional flux at any point of observation as well as the unidirectional fluence which corresponds to the average of the flux along the trajectory of a satellite. The model for the angular distributions of proton fluxes present below are based on different ingredients:

1. an empirical model for the omnidirectional proton flux such as AP-8 MIN or AP-8 MAX models;
2. a model for the pitch-angle distribution;
3. a model for the East-West asymmetry;
4. a method of normalisation.

To evaluate the unidirectional fluence, one has first to define the attitude of the satellite along its orbit. Let $(\bar{1}_u, \bar{1}_v, \bar{1}_w)$ be a coordinate system attached to the satellite. The attitude of the satellite is defined, for instance, by the Euler angles of the coordinate system $(\bar{1}_u, \bar{1}_v, \bar{1}_w)$ with respect to a geographical coordinate system, e.g. $(\bar{1}_x, \bar{1}_y, \bar{1}_z)$ defined in Fig. 1.1 (page 4).

The fluence can be highly anisotropic for a look direction in the satellite frame. Especially for satellites located on a low-altitude orbit where radiation exposure is mainly confined in the region of the South Atlantic Anomaly. For instance, the fluence experienced by a satellite is anisotropic when

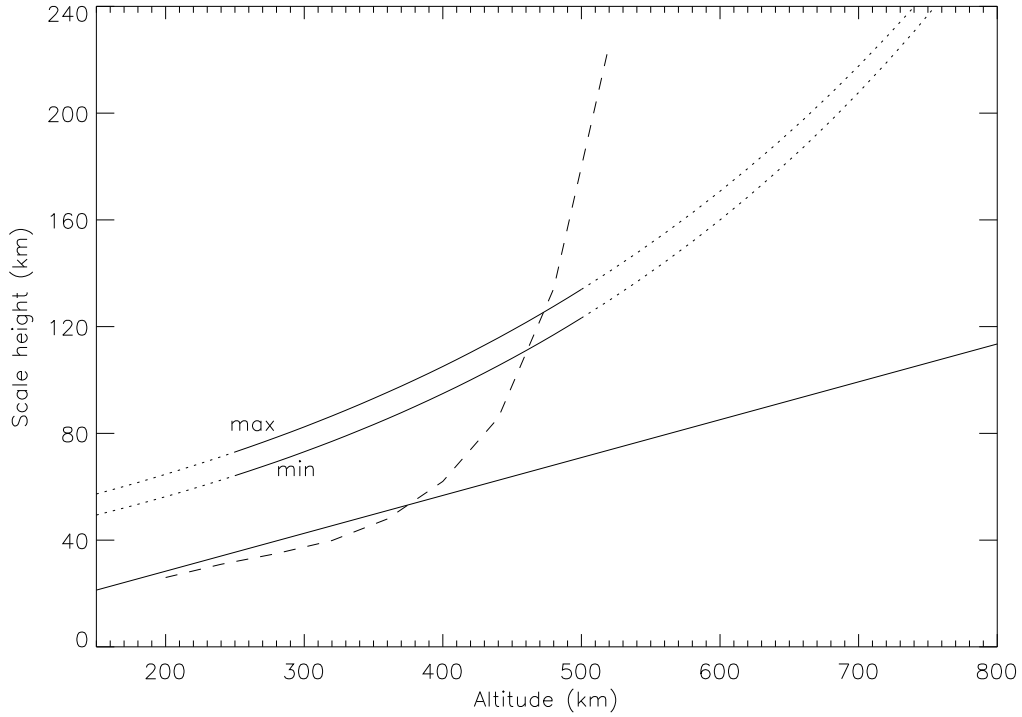

Figure 2.1. Comparison between different scale heights. The dotted-partly-solid lines represent effective scale heights $H^{\min}$ and $H^{\max}$ used by Armstrong et al. (1990) and given in Eqs. (2.1) and (2.2). The solid line is the scale height obtained from Allen's (1985) atmosphere model. The dashed line correspond to the stopping-power scale height as a function of $h_{\widetilde{m}}$ (Heckman and Brady, 1966).

- one of the axis attached to the satellite is aligned along the velocity vector (trailing side compared to leading side),
- one of the axis attached to the satellite is aligned along the gravity gradient (mean magnetic field direction compared to a perpendicular direction),
- the satellite is stabilized with respect to an inertial frame (direction pointing to the geomagnetic East in the South Atlantic Anomaly region compared to the direction pointing to the geomagnetic West).

In this chapter, we describe first the model of Armstrong et al. (1990). In a second part we define and describe a model based on the Badhwar & Konradi (1990) pitch-angle distribution combined with the Lenchek & Singer (1962) model for the East-West asymmetry. Finally, the total angular distributions of proton fluxes and fluences predicted by both of these models are shown and compared.

2.1 Armstrong and Watts models

Armstrong et al. (1990) applied the model for angular distribution developed by Watts et al. (1989) for the AP-8 MIN and MAX model to evaluate differential energy spectra of trapped proton unidirectional fluxes at low altitude. The assumptions on which this model is based have been discussed in another section. The energy spectra presented by these authors were averaged over circular orbits with a 28.5° inclination and an altitude ranging from 300 to 500 km. To analyse the radiation environment of the Space Station, Armstrong et al. (1990) converted the energy spectra to Silicon and BFO* doses using Burrell's (1964) one-dimension proton transport code. To compare their prediction with data from the Long Duration Exposure Facility (LDEF), Armstrong et al. (1992b) also developed a three-dimensional transport calculation based on the HETC† code (Armstrong and Chandler, 1972). The comparison showed that AP-8 underestimates the LDEF data by about a factor of 2 and that the Watts et al. (1989) model produces weaker anisotropies than those observed. This latter discrepancy can be attributed to the inappropriate atmospheric scale height used in Armstrong et al.'s (1990) calculation.

In this section, we describe the trapped proton anisotropy model which was labelled VF1MIN and VF1MAX by Colborn, Armstrong and Watts (1990). VF1 stands for Vector Fluxes, version 1. The VF1MIN and VF1MAX models correspond to solar minimum and solar maximum. In these models, conversion factor, to transform omnidirectional flux into unidirectional flux, is given by

$$W_{\mathrm{VF}}(E,\alpha,\phi) = \frac{\exp\left(-\dfrac{(\pi/2-\alpha)^2}{2\sigma^2}\right)}{\sin\alpha\sqrt{2\pi}\sigma\,\mathrm{erf}\left(\dfrac{\pi}{\sqrt{8}\sigma}\right)} \frac{\exp\left(\dfrac{\widetilde{r}_{\mathrm{g}}\cos I\cos\beta(\alpha,\phi)}{H}\right)}{\displaystyle\int_0^{2\pi}\exp\left(\frac{\widetilde{r}_{\mathrm{g}}\cos I\cos\beta(\alpha,\phi)}{H}\right)\mathrm{d}\phi} \tag{2.1}$$

which is deduced from Eq. (1.36). The omnidirectional spectra $j_0(E)$ at solar minimum and solar maximum are taken from the AP-8 MIN and MAX models respectively. Colborn et al. (1990) have used the atmospheric scale height H obtained from the Johnson and Smith (1985) atmospheric model: H is an increasing function of the altitude which has been approximated for solar minimum and maximum by

$$H^{\min} = 33.4\mathrm{km}\times\exp\left(\frac{h}{383\mathrm{km}}\right), \tag{2.2}$$

$$H^{\max} = 39.8\mathrm{km}\times\exp\left(\frac{h}{412\mathrm{km}}\right). \tag{2.3}$$

*Blood Forming Organs (BFO)

†High-Energy Transport Code (HETC)

The expressions (2.2) and (2.3) are assumed to be valid in an altitude range between 250 and 500 km. Within this study, we have reconstructed the models VF1MIN and VF1MAX from the Eqs. (2.1), (2.2) and (2.3) where the integral in the denominator of (2.1) is evaluated by the expansion series given by Eq. (1.35).

In Fig. 2.1, Colborn et al. (1990) scale heights are compared to the atmospheric scale height $H(h)$ based on Allen's (1985) atmosphere model‡ [see Eq. (1.22)] and Heckman & Brady's (1966) effective scale height $H_{\Delta E}$ based on the energy loss by a particle along its trajectory [see Eq. (1.49)]. The atmospheric scale height $H(h)$ (full solid line) and Colborn et al. (1990) effective scale heights $H^{\min}$ and $H^{\max}$ (dotted - partly - solid lines) are functions of the altitude h. The Heckman & Brady's (1966) effective scale height $H_{\Delta E}$ (dashed line) has been determined for a set of drift shells $(B_{\rm m}, L_{\rm m})$ where $L_{\rm m}$ is fixed at 1.38 and where $B_{\rm m}$ varies from 0.2043 to 0.2355 gauss. The effective energy loss scale height $H_{\Delta E}$ is a function of the lowest mirror point altitude $h_{\widetilde{\rm m}}$.

The shapes of the solar minimum and solar maximum Armstrong's scale heights are similar. The difference between $H^{\min}$ and $H^{\max}$ does not exceed 11 km in the altitude range 250–500 km. In that altitude range, $H^{\min}$ and $H^{\max}$ are about 45 km larger than Allen's (1985) atmospheric scale height given by Eq. (1.22). Additional atmospheric models can, of course, also be used to determine this latter local density scale height. It can be seen that the altitude distribution of the effective scale height $H_{\Delta E}$ is quite different from all others. Below 350 km, $H_{\Delta E}$ is almost equal to the local atmospheric scale height of Allen's (1985) model. At these altitudes, the main constituents of the atmosphere are N_2, O_2 and O which have almost the same ratio A/Z. Therefore the rate of energy loss is proportional to the atmospheric density. Above 350 km, Heckman and Brady's (1966) effective scale height increases very sharply, indeed the abundance of Helium and Hydrogen is increasing about this height. As a matter of consequence, the ionization energy losses are no longer proportional to the total atmospheric density.

Note that $H_{\Delta E}$ is a function of $B_{\rm m}$ and $L_{\rm m}$; it is not a function of the altitude of the point of observation. For instance, when an observer is located at different positions corresponding to $B_{\rm m}$ =0.2230 gauss and $L_{\rm m}$ =1.38, the altitude of his actual position may vary from 326 to 1,670 km but the effective scale height $H_{\Delta E}$ will be constant and equal to 41 km. On the contrary according to expression (2.3), at 326 km the scale height $H^{\max}$ will be about 88 km while at 1,670 km it will be larger than 2,000 km!

‡For the purpose of this comparison, a simple atmospheric model is good enough. Allen's (1985) atmospheric model does not include parameters [see Eq. (1.22)] and is based on COSPAR International Reference Atmosphere (CIRA, 1965). It provides a good order of magnitude estimate for the altitude dependence of the atmospheric density. The more realistic semi-empirical model MSIS (Hedin, 1987 and 1991) may also be used.

Table 2.1. Values of the parameters relative to BK-MIN and BK-MAX trapped proton flux anisotropy models

Model	H	p_1	p_2	p_3	p_4
BK-MIN	100.0	−0.032392	0.039836	0.13164	−8.8674
BK-MAX	100.0	−0.031690	0.039119	0.09294	−6.1651

Since Armstrong et al. (1990) restrict their model to the altitude range between 250 and 500 km, trapped proton are only observed in the South Atlantic Anomaly, where the mirror points are the lowest ones. When the observer is not near the position of a lowest mirror point, the drift shell generally hit the Earth's surface in the vicinity of the South Atlantic Anomaly. Therefore, when Armstrong et al. (1990) model is supposed to become inadequate, the radiation flux of proton is vanishingly small. However, their model provides a reasonable values of the scale height of pitch-angles close to 90°, i.e. where the directional flux of proton is maximum.

Examples of results obtained with the VF1MIN model will be presented in Sect. 2.3 and 2.4.

2.2 Application of Badhwar and Konradi model

As shown in Sect. 1.2.4, the Heckman and Nakano (1969) pitch-angle distribution does not reproduce experimental data in the vicinity of the loss cone angle. The inaccuracy of this theoretical approach is mainly due to the lack of a loss cone and to the use of a local scale height (see Sect. 1.4.4) instead of an effective one.

To evaluate the effects of the pitch-angle distribution on the orbit-averaged trapped proton flux anisotropy, we define two very simple models based on the Badhwar and Konradi (1990) pitch-angle distribution. The models will be called BK-MIN and BK-MAX, respectively for solar minimum and solar maximum conditions.

In these models, the anisotropy conversion factor, to transform omnidirectional flux into unidirectional flux, is deduced from Eqs. (1.17), (1.25) with a global normalisation (see Sect. 1.4.1). When $\alpha_{\mathrm{L}} < \alpha < \pi - \alpha_{\mathrm{L}}$, it is given by

$$W_{\mathrm{BK}}(E,\alpha,\phi) = \frac{\dfrac{\sin\alpha - \sin\alpha_{\mathrm{L}}}{\sqrt{B}} \exp\left(-b\dfrac{\sin\alpha - \sin\alpha_{\mathrm{L}}}{\sqrt{B}}\right) \exp\left(\dfrac{\widetilde{r}_{\mathrm{g}} \cos I \cos\beta(\alpha,\phi)}{H}\right)}{4\pi \displaystyle\int_{\alpha_{\mathrm{L}}}^{\pi/2} \left[\mathrm{I}_0\left(\frac{\widetilde{r}_{\mathrm{g}} \cos I \sin\alpha'}{H}\right) \frac{\sin\alpha' - \sin\alpha_{\mathrm{L}}}{\sqrt{B}} \exp\left(-b\frac{\sin\alpha' - \sin\alpha_{\mathrm{L}}}{\sqrt{B}}\right)\right] \mathrm{d}\cos\alpha'} \,. \quad (2.4)$$

Otherwise, the conversion factor is given by

$$W_{\mathrm{BK}}(E, \alpha, \phi) = 0\,.$$

The integral in Eq. (2.4) is evaluated numerically by a Gauss-Legendre quadrature. The loss-cone angle α_{L} is related to the equatorial loss-cone angle α_{L0} by the conservation of the magnetic moment [see Eq. (1.40)]:

$$\sin \alpha_{\mathrm{L}} = \sqrt{\frac{B}{B_0}} \sin \alpha_{\mathrm{L0}} \tag{2.5}$$

When, at the location of observation, B is greater than $B_0 / \sin^2 \alpha_{\mathrm{L0}}$, the trapped protons are absorbed by the atmosphere and the proton flux is set equal to zero.

The equatorial loss-cone pitch angle α_{L0}, the slope parameter b and scale height H are functions of the drift shell parameter L. For the sake of simplicity, H is set to a constant value and the parameters α_{L0} and b are defined as functions of L.

The parameters α_{L0} and b are obtained from the fit of the distribution f_{BK} to the AP-8 unidirectional fluxes of 20 MeV trapped protons. The parameters are closely approximated by the expressions:

$$\alpha_{\mathrm{L0}}^{-1} = p_1 + p_2 L \tag{2.6}$$

$$b^{-1} = p_3 + p_4 \ln L \tag{2.7}$$

where α_{L0} is expressed in degrees and b in gauss$^{\frac{1}{2}}$. The values of the scale height and of the different parameters p_1, p_2, p_3 and p_4 are given in Table 2.1 for solar minimum and maximum condition. The parameters p_1, p_2, p_3 and p_4 were evaluated for 20 MeV protons; their values vary slightly with the proton energy.

Examples of results obtained with the BK-MIN model will be presented in Sect. 2.3 and 2.4.

2.3 Predicted angular distribution

Two examples of angular distribution obtained with the VF1MIN and BK-MIN models are presented in Figs. 2.2, 2.3, 2.5 and 2.6. They correspond to the differential trapped proton flux predicted at two different points of observation $\bar{p}$ and $\bar{q}$ in the South Atlantic Anomaly. Their altitude is respectively 450 and 1,500 km. Both points are located at 60°W and 35°S.

The space coordinate system used is orthogonal and defined such that

– the z-axis points to the zenith (corresponds to $\bar{1}_R$ in Fig. 1.1);

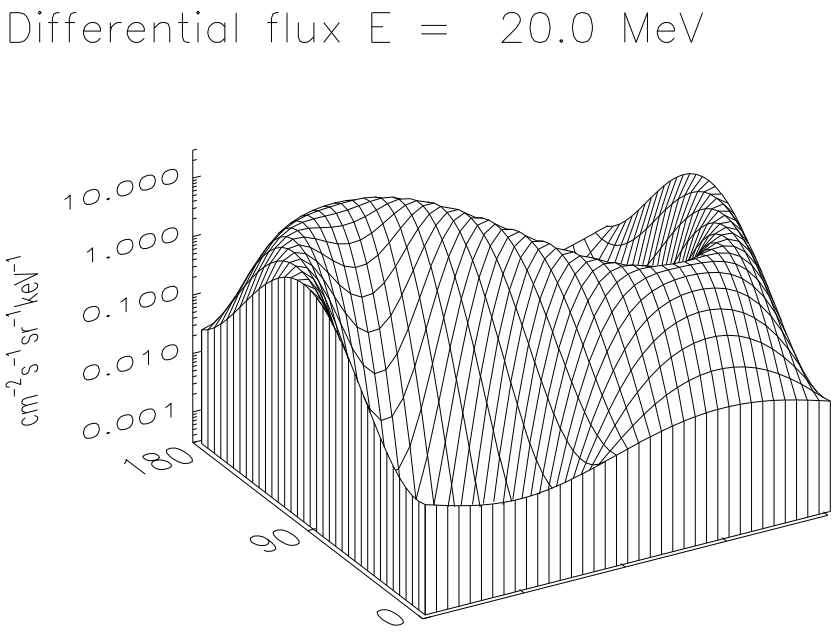

Figure 2.2. VF1MIN predicted anisotropy of trapped proton differential flux at 60°W, 35°S and altitude 450 km based on the model. The proton energy is set to 20 MeV and the omnidirectional flux is fixed to $12.5\,\mathrm{cm^{-2}s^{-1}keV^{-1}}$. The coordinate system is fixed relatively to the zenith direction (z-axis) and the local magnetic East direction.

- the y-axis lies at the intersection of the mirror plane and the horizontal plane; it points in the eastward direction (corresponds to $\bar{1}_y$ in Fig. 1.1);
- the x-axis is defined by the intersection between the mirror plane and the local vertical plane which contains the magnetic field line (corresponds to $\bar{1}_H$ in Fig. 1.1).

The proton energy is $E = 20\,\mathrm{MeV}$ and the omnidirectional differential flux is equal to $12.5\,\mathrm{cm^{-2}s^{-1}keV^{-1}}$. The Jensen and Cain (1962) geomagnetic field model was used to obtain the (B, L) coordinates.

The magnetic coordinates (B, L), the magnetic dip angle I, the parameter σ, the scale height $H^{\min}$ and the Badhwar & Konradi loss cone angle α_{L} are given in Table 2.2.

2.3.1 Angular distribution at 450 km altitude

The predicted angular distributions observed at the point $\bar{p}$ corresponding to an altitude of 450 km are presented in Figs. 2.2 and 2.3, respectively for the VF1MIN and

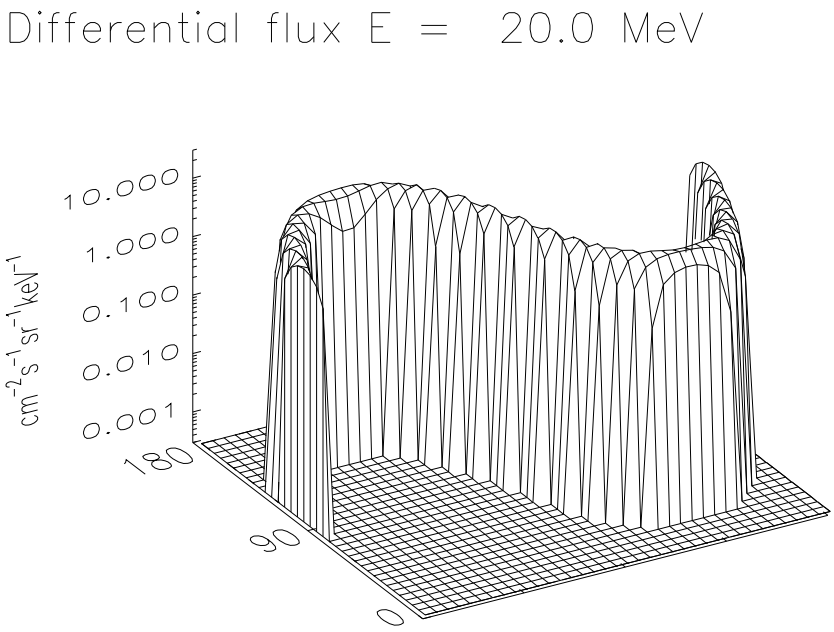

Figure 2.3. BK-MIN predicted anisotropy of trapped proton differential flux at 60°W, 35°S and altitude 450 km. The proton energy is set to 20 MeV and the omnidirectional flux is 12.5 $\mathrm{cm^{-2}s^{-1}keV^{-1}}$. The coordinate system is fixed relatively to the zenith direction (z-axis) and the East direction.

Table 2.2. Magnetic coordinates (B, L), magnetic dip angle I, parameter σ and scale height $H^{\min}$ for two points of observation . The (B, L) coordinates are obtained using the Jensen and Cain (1962) geomagnetic field model.

location	B (gauss)	L	I (deg)	σ (deg)	$H^{\min}$ (km)	α_{L} (deg)
60°W, 35°S, 450 km	0.2210	1.28	33.6	10.3	108.1	79.5
60°W, 35°S, 1500 km	0.1551	1.47	35.2	37.4	1677.2	51.0

BK-MIN models. The unidirectional differential fluxes are presented as a function of the polar and azimuthal angles. It can be seen that the angular variations of the unidirectional differential flux are quite different in Figs. 2.2 and 2.3. In Fig. 2.2, the angular distribution has two deep valleys centred respectively around the polar angles 56°, 124° and azimuthal angles 90°, 270°. These two directions correspond to the directions of the magnetic field line. The angular distribution found with the BK-MIN model and shown in Fig. 2.3 is much steeper than that corresponding to the VF1MIN model and looks like a sheer ridge. In other words, a narrower angular

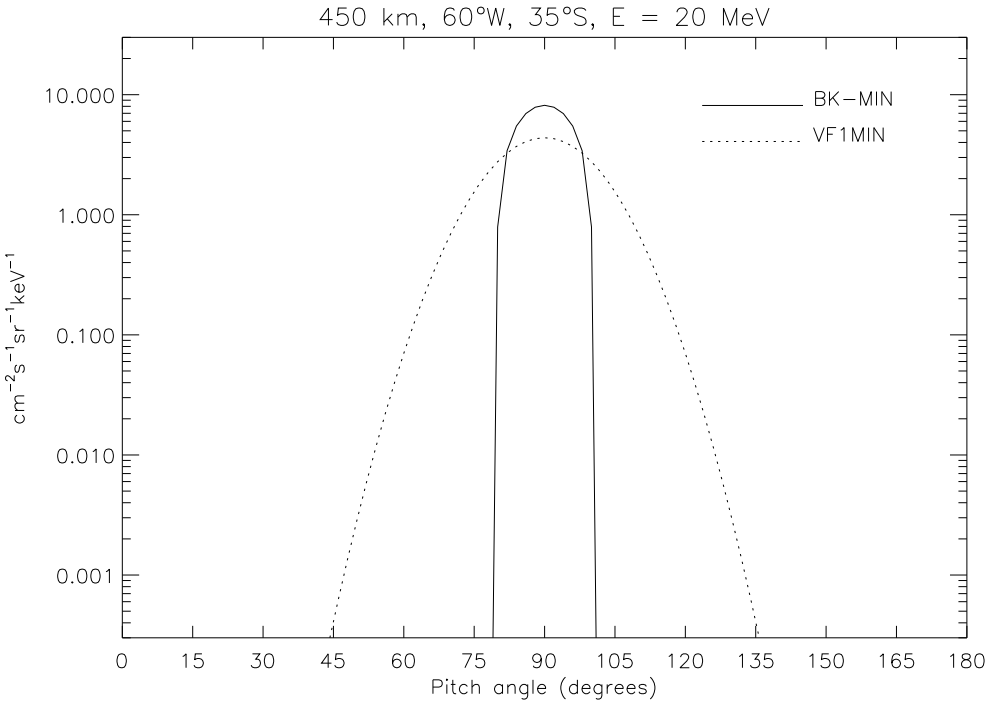

Figure 2.4. Comparison of the pitch-angle distributions obtained from the models VF1MIN and BK-MIN at 60° W, 35°S and altitude 450 km. The figure presents the unidirectional differential fluxes of protons in the vertical plane containing the magnetic field direction. The omnidirectional flux is 12.5 $\mathrm{cm^{-2}s^{-1}keV^{-1}}$.

distribution is obtained with the BK-MIN model than with the VF1MIN model.

The pitch-angle distribution of both models are compared in Fig. 2.4. Figure 2.4 gives the unidirectional fluxes for 20-MeV protons obtained from the models VF1MIN (dotted line) and BK-MIN (solid line) in the vertical plane $(\bar{1}_B, \bar{1}_x)$ of Fig. 1.1 on page 4. The pitch-angle distribution of the model BK-MIN is more sharply peaked than the one corresponding to the model VF1MIN.

In the BK-MIN model, based on Badhwar and Konradi's (1990) approximation, the loss cone is defined explicitly by the means of the α_{L} angle. At the point $\bar{p}$, α_{L} =79.5° and the unidirectional flux is confined to a cone of 21° opening angle. On the other hand, within the Heckman and Nakano (1969) description used in the VF1MIN model, the loss cone is defined implicitly through the parameter[§] σ. At the point $\bar{p}$, σ =10.3° which induces a smoother anisotropy than the Badhwar and Konradi (1990) pitch-angle distribution as shown in Fig. 2.4. At α =90°, the

[§]The pitch-angle distribution is described with the help of a gaussian of which σ is the half-width parameter (see Sect. 1.2.2).

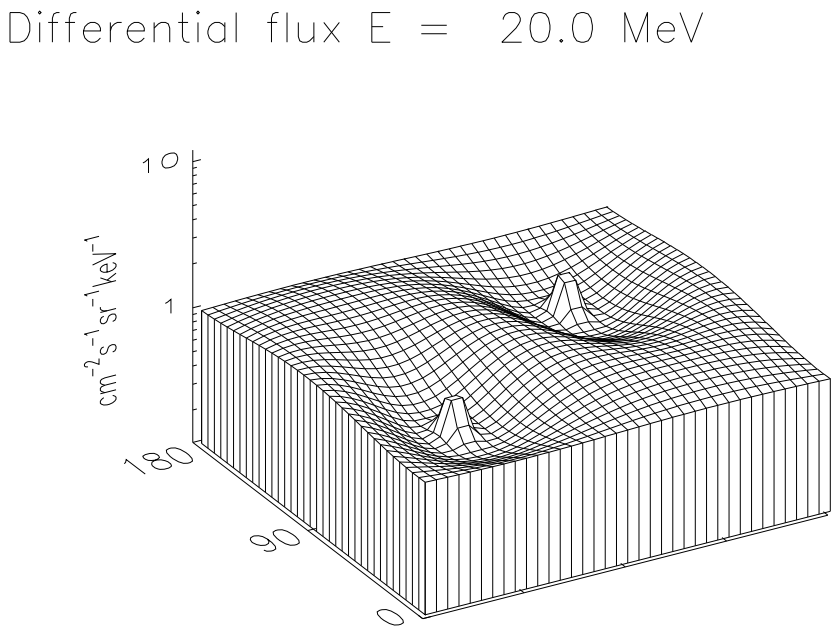

Figure 2.5. Same as Fig. 2.2 but for an altitude of 1500 km based on the VF1MIN model.

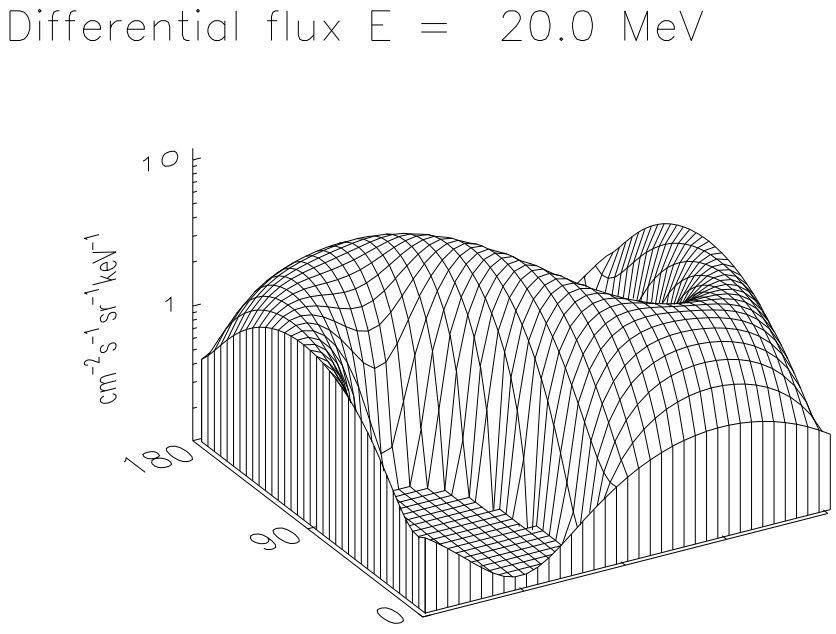

Figure 2.6. Same as Fig. 2.3 but for an altitude of 1500 km based on the BK-MIN model.

differential flux predicted by the VF1MIN model is lower than this predicted by the BK-MIN model due to the normalisation with respect to the omnidirectional flux [see Sect. 1.4, Eq. (1.27)].

Since the parameter α_L is obtained from a fit of the AP-8 MIN unidirectional flux database (see Sect. 1.2.4), the results obtained with the BK-MIN model is a better approximation for the AP-8 MIN trapped proton model than those obtained with the VF1MIN model.

2.3.2 Angular distribution at 1,500 km altitude

The angular distributions of the unidirectional differential flux predicted at second point $\bar{q}$ are presented in Figs. 2.5 and 2.6, respectively for the VF1MIN and BK-MIN models. The altitude of $\bar{q}$ is 1,500 km. The shape of the angular distribution for both models is quite different from that for altitude 450 km illustrated in Figs. 2.2 and 2.6.

The valleys in Fig. 2.5 are shallower than in Fig. 2.2 as a result of increase of the parameter σ from 10.3° to 37.4°. However, unexpected peaks appear in the center of both valleys. The two peaks correspond respectively to pitch-angles of 0° and 180°! They are caused by the singularity in the conversion factor W_{VF} of Eq. (2.1). Indeed, when $\sin\alpha$ tends to zero, Expression (2.1) diverges. The singularity is a consequence of the particular normalisation method chosen by Watts et al. (1989) [see Eq. 1.34]. This divergence should have appeared already at the lower altitude ($\bar{p}$): i.e. in Fig. 2.2 where σ =10.3°. But in this case the value of the gaussian $\exp[-(90° - \alpha)^2/2\sigma^2]$ in Eq. (2.1) becomes very small when α is near 0° or 180°; therefore the divergence of W_{VF} is masked as a result of the grid mesh. On the contrary, at $\bar{q}$ where σ =37.4°, the value of the gaussian is much larger and the divergence of Eq. (2.1) is emphasized; therefore the two peaks clearly appear in the directions parallel and anti-parallel to the magnetic field direction.

At low altitude where the parameter σ is small, this singularity does not appear. As a consequence when the altitude of observation exceeds 1,000 km the VF1MIN and VF1MAX models should not be used.

In the BK-MIN model, the extension to a higher altitude does not cause any problems. The loss cone angle at the point $\bar{q}$ is about 51° and the ridge seen in Fig. 2.3 flattens out in Fig. 2.6. In other words, the pitch-angle distribution and the East-West asymmetry become less anisotropic. However, the fact that two deep holes remain proves that at 1,500 km altitude, the anisotropy of the trapped proton flux is still important.

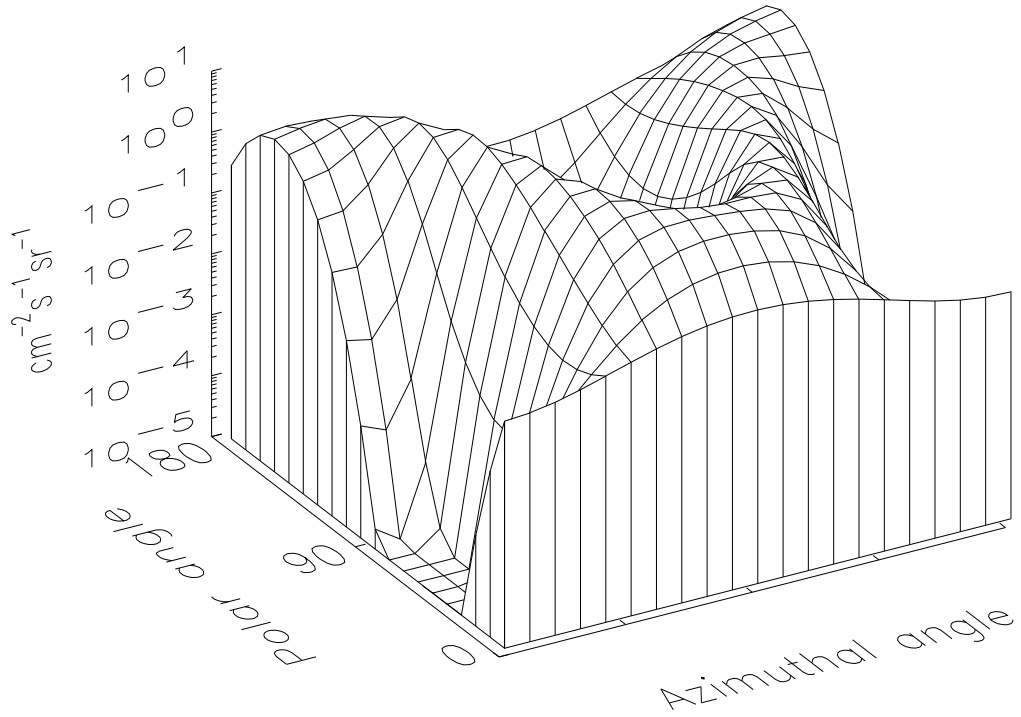

Figure 2.7. Anisotropy of trapped proton integral flux (E >100 MeV) averaged over a circular orbit, 28.5° inclination, 450 km predicted by the VF1MIN model. The satellite orientation and the direction of the detector are fixed with respect to the zenithal direction and the North direction in the horizontal plane.

2.4 Prediction of proton fluence

Examples of trapped proton fluences obtained with the VF1MIN and BK-MIN models are presented in Figs. 2.7, 2.8, 2.9 and 2.10. They correspond to the integral fluence (E >100 MeV) obtained from an average over twelve successive circular orbits at 450 km altitude and 28.5° inclination. The satellite orientation is fixed with respect to the zenithal direction and to the geographic North direction in the horizontal plane. The omnidirectional proton spectra are taken from the AP-8 MIN model. The parameters (B, L) along the orbit are computed using the Jensen and Cain (1962) geomagnetic field model which must be attached to the AP-8 MIN radiation belt model. The omnidirectional integral fluence at E >100 MeV, averaged over the twelve orbits, is equal to 13.04 $cm^{-2}s^{-1}$.

The results obtained with the Armstrong et al. (1990) model VF1MIN are presented in Figs. 2.7 and 2.8. The results may be slightly different that Armstrong et al. (1990) published results due to different geomagnetic field models and therefore

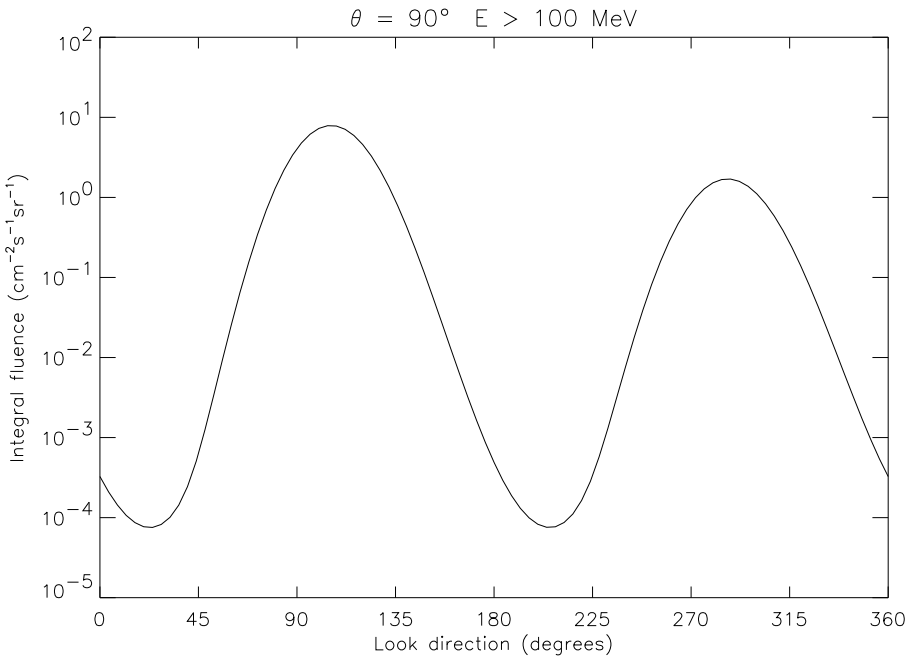

Figure 2.8. Angular variation of trapped proton integral flux (E >100 MeV) averaged over a circular orbit, 28.5° inclination, 450 km predicted by the VF1MIN model. The satellite orientation and the direction of the detector are fixed with respect to the zenithal direction and to the North direction in the horizontal plane.

different values of McIlwain's (1965) B and L coordinates.

In Fig. 2.7, the integral fluence is given as a function of the look direction $\bar{D}$ i.e. the direction of the detector. When the fluence is numerically integrated over all look directions, the omnidirectional integral fluence obtained is equal to $12.95\,\mathrm{cm^{-2}s^{-1}}$ which is slightly different from the initial value of $13.04\,\mathrm{cm^{-2}s^{-1}}$ (see discussion at Sect. 3.3.1). This mirror difference may be attributed to numerical integration errors. The unidirectional integral fluence varies significantly with the polar and azimuthal angles. The mean value of the unidirectional integral fluence is about $1\,\mathrm{cm^{-2}s^{-1}sr^{-1}}$. The two "holes" (up-North and down-South zones) correspond to directions of the upward and downward loss cone.

In Fig. 2.8, the angular distribution of the integral fluence in the horizontal plane is presented and shows clearly the East-West effect. Proton integral fluence seen from the West direction (∼105°) is higher than the flux seen from the East direction (∼285°). Indeed, protons coming from the West have their guiding centres above the point of observation, while the protons coming from the East have their guiding centres below the point of observation (Lenchek and Singer, 1962). The West/East ratio of the incident trapped proton integral flux (E >100 MeV) is about

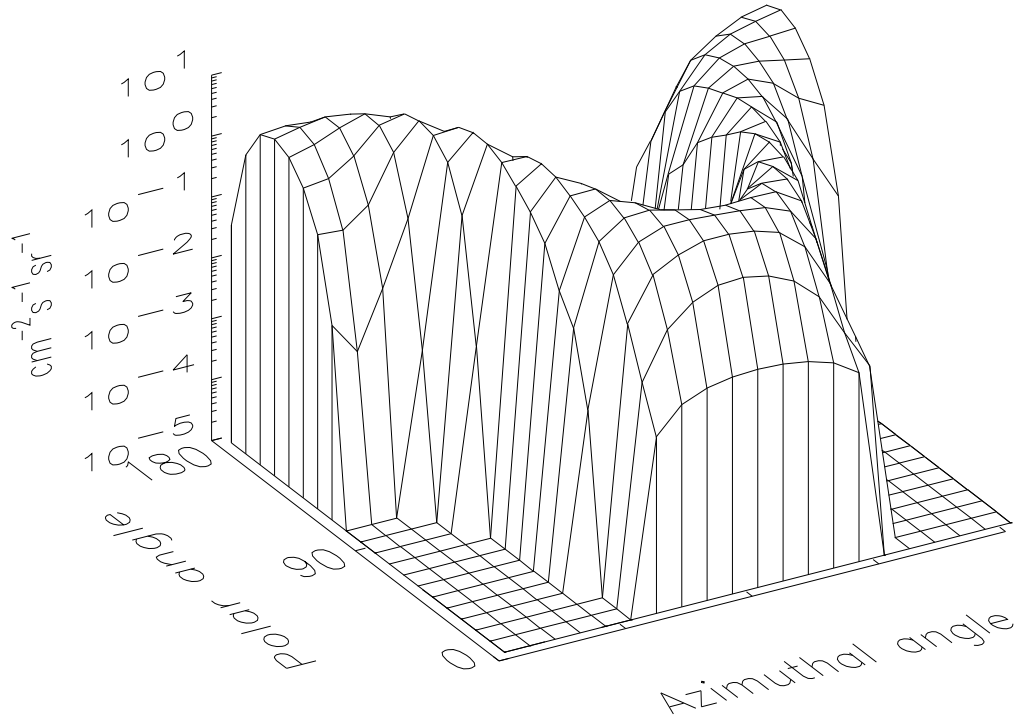

Figure 2.9. Anisotropy of proton integral flux (E >100 MeV) averaged over a circular orbit, 28.5° inclination, 450 km predicted with the BK-MIN model. The satellite orientation and the direction of the detector are fixed relatively to the zenithal direction and the North direction in the horizontal plane.

4.64.

The results corresponding to the BK-MIN model are presented in Figs. 2.9 and 2.10.

In Fig. 2.9, the omnidirectional integral fluence, obtained by numerical integration, is equal to 13.37 $cm^{-2}s^{-1}$ which is slightly larger than the initial value of 13.04 $cm^{-2}s^{-1}$. As expected, the unidirectional fluence anisotropy obtained by the model BK-MIN is higher than that corresponding to the VF1MIN model which is shown in Fig. 2.7. This feature was already highlighted in the previous section.

The differences in the anisotropy predicted by both models appears more clearly when the angular variation in the horizontal plane are compared as in Figs. 2.8 and 2.10. The peaks obtained by the BK-MIN model are sharper than those obtained by VF1MIN: in the BK-MIN model, the trapped proton flux drops to zero in the loss cone directions. In Fig. 2.10, the West/East ratio of the incident trapped proton integral flux (E >100 MeV) is about 5.15 which is larger than the corresponding ratio of Fig. 2.8. The difference is due to different atmospheric scale heights used

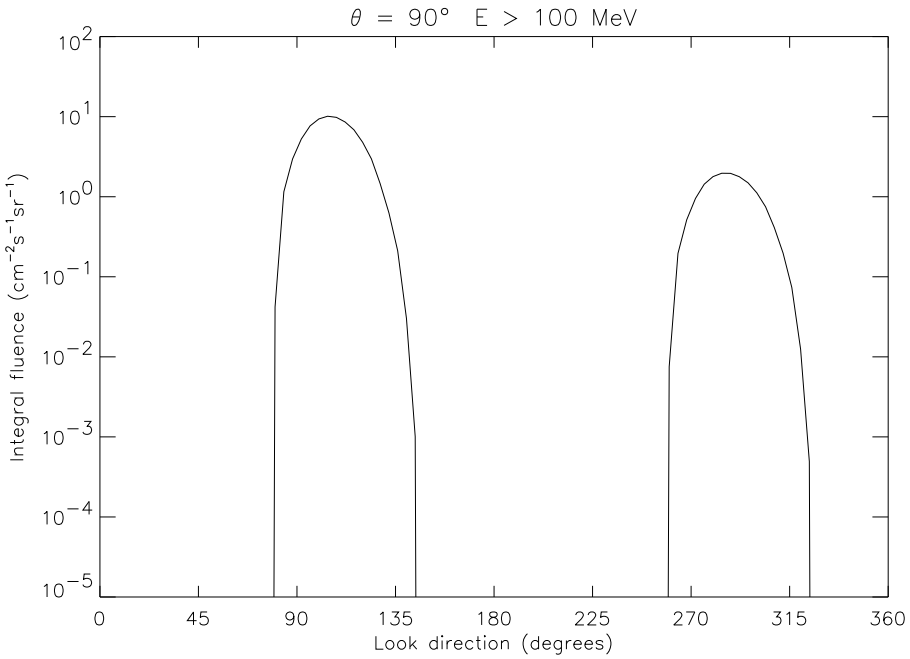

Figure 2.10. Angular variation of trapped proton integral flux ($E > 100$ MeV) averaged over a circular orbit, 28.5° inclination, 450 km predicted with BK-MIN model. The satellite orientation and the direction of the detector are fixed relatively to the zenithal direction and to the North direction in the horizontal plane.

in both models. At 450 km, the scale height of the VF1MIN model is about 500 km while it is fixed at 100 km in the BK-MIN model.

The unidirectional trapped proton fluences may be used as an input to one-dimensional shielding model `SHIELDOSE` (Seltzer, 1979). It can also be used to determine the anisotropic distribution of the radiation dose inside a spacecraft using a three-dimensional shielding model as it is done by Armstrong and Chandler (1972).

Chapter 3

Implementation of ANISO

The software package UNIRAD (Heynderickx and Lemaire, 1995) is a suite of programs developed for ESA for evaluating the radiation fluences and doses experienced by a spacecraft along its orbit.

This chapter is devoted to the implementation of the trapped proton anisotropy models in the UNIRAD package. This implementation consists mainly in a program called ANISO which allows to calculate the trapped proton unidirectional fluences observed for a given orbit and a given direction $\bar{D}$ of the detector view angle, both are input parameters specified by the user.

The unidirectional fluences are obtained by the transformation of the omnidirectional differential flux into an unidirectional flux along the orbit. The unidirectional differential flux is then averaged over the whole orbit to provide an unidirectional fluence.

After a short review of the existing UNIRAD package, the implementation of ANISO will be described. A sample run of the ANISO program will be presented.

The specifications and user requirements of ANISO as well as a top-down description of software requirements and architecture are included in the URD and SRD documents given in the Appendices A and B respectively.

3.1 Overview of UNIRAD

The UNIRAD package (Heynderickx and Lemaire, 1995) includes an orbit generator (SAPRE), a program to calculate McIlwain's (1961) B and L coordinates (BLXTRA), another program to calculate the omnidirectional flux of trapped protons and electrons (TREP), and a program to convert the energy spectra to radiation dose (SHIELDOSE). The different UNIRAD programs are controlled by a Fortran namelist file PROJECT.NML which consists of a sequence of namelists specific for each of these programs. Data

Table 3.1. List of UNIRAD interface files

File ext.	Modified by	Used by	Content and remarks
INT	SAPRE, BLXTRA, TREP	TREP, ANISO, BLXTRA	Ephemeris, geomagnetic coordinates, integral flux summary. ASCII File.

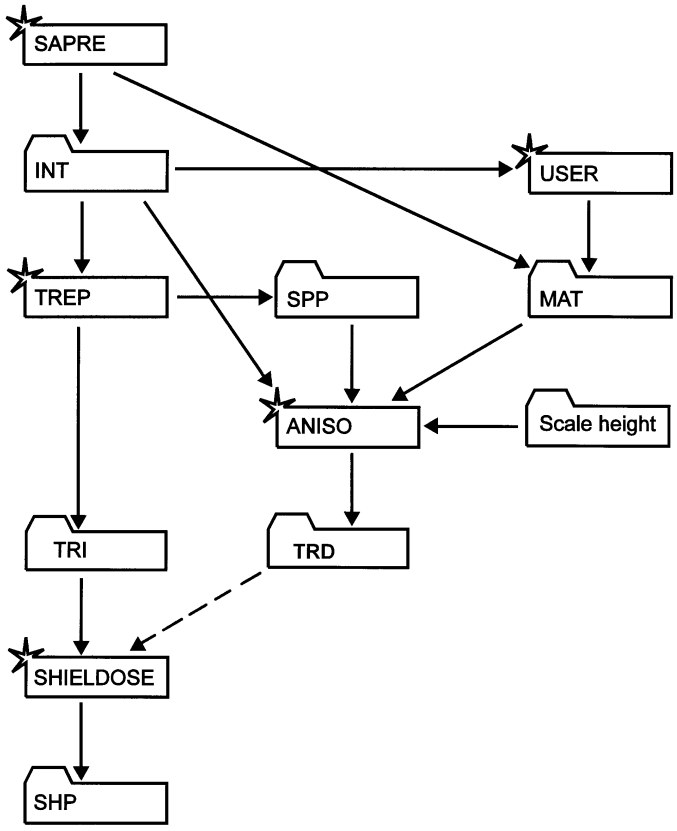

Figure 3.1. Flow diagram of UNIRAD

are exchanged between the programs by the use of interface files.

The different interface files are listed in Table 3.1. The programs TREPPOS, TREPAVE, EQFRUX and EQFRUXGA are part of the UNIRAD package. The ANISO implementation requires as data the files PROJECT.INT, PROJECT.SPP and PROJECT.MAT. The first two were already produced by the existing programs. The last one, describing the satellite attitude has to be provided by the user. The SAPRE program has be adapted to generate a default PROJECT.MAT file. The ANISO program produces the

Table 3.2. Record structure of the interface file PROJECT.MAT determining the attitude of particle detector or the view angle directions

Word	Data Type	Description
1–9	REAL*8	Rotation matrix describing the satellite attitude relative to the geographic spherical axis $(\bar{1}_R, \bar{1}_\theta, \bar{1}_\phi)$ at the current location of the satellite
10	REAL*8	Angle between the zenith direction and the satellite velocity vector (degrees)

PROJECT.TRD file which contains unidirectional trapped proton fluences.

The implementation of ANISO does not modify the use of UNIRAD when the East-West anisotropy is bypassed. Part of the flow diagram of the new UNIRAD package is represented in Fig. 3.1. This diagram illustrates the interdependence between different program elements. The original set of UNIRAD programs has been grouped on the left hand part of the diagram. Except for PROJECT.SHP, the other output files are not shown. The right hand part of the diagram corresponds to the inputs and output of the ANISO program. The PROJECT.INT and PROJECT.MAT files contain the ephemeris and attitude of the satellite or view angles of the particle detectors. The magnetic field vector and the omnidirectional integral fluxes are provided to ANISO through the PROJECT.SPP file generated by TREP. The output file PROJECT.TRD contains the orbit averaged unidirectional integral and differential fluences. The structure of the file PROJECT.TRD is similar to that of the file PROJECT.TRI and is described in Table 3.4.

3.2 Attitude interface file

. The attitude interface file PROJECT.MAT is an input of ANISO which contains the attitude of the satellite along its orbit. This file may be generated by SAPRE for the three cases listed in Sect. 3.2.1. For other cases, the file PROJECT.MAT must be produced by the user as an input.

The attitude interface file PROJECT.MAT is in Fortran unformatted format, with fixed record length of 80 bytes, in direct access. Each record corresponds to an orbital point in the common interface file (PROJECT.INT). The structure of the attitude

interface file is given in Table 3.2. The rotation matrix is given by

$$[A(i,j)] = \begin{bmatrix} \bar{1}_R \cdot \bar{1}_x & \bar{1}_R \cdot \bar{1}_y & \bar{1}_R \cdot \bar{1}_z \\ \bar{1}_\theta \cdot \bar{1}_x & \bar{1}_\theta \cdot \bar{1}_y & \bar{1}_\theta \cdot \bar{1}_z \\ \bar{1}_\phi \cdot \bar{1}_x & \bar{1}_\phi \cdot \bar{1}_y & \bar{1}_\phi \cdot \bar{1}_z \end{bmatrix} \tag{3.1}$$

where $(\bar{1}_x, \bar{1}_y, \bar{1}_z)$ is the coordinate system attached to the satellite and $(\bar{1}_R, \bar{1}_\theta, \bar{1}_\phi)$ is the geocentric spherical coordinate system. The unit vector $\bar{1}_R$ points to the zenith. The unit vectors $\bar{1}_\theta$ and $\bar{1}_\phi$ lie in the horizontal plane, pointing respectively to the geographic South and East directions.

3.2.1 Changes implemented in the SAPRE program

The `SAPRE` program has been modified to generate simple attitude interface files. This new feature is controlled by the new namelist parameter `IATTI` (`INTEGER*4`). The default value is set to 0; in this case no attitude interface file is generated. When `IATTI` is set to a positive value, a `PROJECT.MAT` file is generated by `SAPRE`. The file contains the attitude of the satellite which corresponds to one of the 3 orientations of the satellite:

`IATTI` =**1** The z-axis of the satellite points to the zenith. The x-axis and y-axis are in the horizontal plane pointing respectively to the geographic North and West directions. This satellite attitude was used in Sect. 2.4 to illustrate the angular distribution of the unidirectional flux.

`IATTI` =**2** The z-axis is parallel to the velocity vector of the satellite. The x-axis lies in the orbital plane pointing away from the Earth. The y-axis is perpendicular to the orbital plane, pointing to the South.

`IATTI` =**3** The $(\bar{1}_x, \bar{1}_y, \bar{1}_z)$ coordinate system is parallel to the geographic equatorial inertial coordinate system.

When different `SAPRE` namelists are present in the same file `PROJECT.NML`, `IATTI` has to be either equal to zero in every namelist, or always greater than zero. In other words, trajectories with and without `ANISO` calculations should not be mixed.

3.3 ANISO program

The `ANISO` program transforms trapped proton omnidirectional integral fluxes produced by `TREP` into orbit-averaged unidirectional integral and differential fluences. The program may also provide the unidirectional integral or differential fluxes along

Table 3.3. ANISO namelist parameters

Parameter	Type	Default	Function
JANIS	I*4	1	Anisotropy model identification number 1: VF1MIN model (Watts et al., 1990) 2: VF1MAX model (Watts et al., 1990) 3: BK-MIN model (Badhwar and Konradi, 1990) 4: BK-MAX model (Badhwar and Konradi, 1990)
NDIR	I*4	180	Number of look directions (12×15)
DALPH	R*4(400)		Polar angle for each look direction in degrees. Default: DALPH($j+15*i+1$) = $7.5+15i$ where i varies from 0 to 11 and j from 0 to 14.
DBETA	R*4(400)		Azimuthal angle for each look direction in degrees. Default: DBETA($j+15*i+1$) = $24j$ where i varies from 0 to 11 and j from 0 to 14.
XOMEGA	R*4(400)	0	Solid angle for each look direction, in sterradian. When XOMEGA is set to zero, XALPH and XBETA are used as polar and azimuthal opening angle to compute the solid angle; in sterradians.
XALPH	R*4(400)	15	Polar opening angle, in degrees
XBETA	R*4(400)	24	Azimuthal opening angle, in degrees
IFULL	I*4	0	When IFULL is greater than zero, the file PROJECT.SPD is generated.

the orbit of the satellite. The transformation is based on the trapped proton anisotropy models described in Sect. 2.1 and 2.2. The ANISO program takes as input the namelist ANISO, it reads the geodetic and (B, L) coordinates from the common interface file PROJECT.INT, the satellite attitude from the attitude interface file PROJECT.MAT, the magnetic field vector components and the full proton flux spectrum from the file PROJECT.SPP.

The namelist parameters controlling the program ANISO are listed in Table 3.3. The polar and azimuthal angles DALPH and DBETA are defined in the coordinate system $(\bar{1}_x, \bar{1}_y, \bar{1}_z)$ attached to the satellite.

Please note that the trapped proton anisotropy models have to be used with the appropriate omnidirectional spectra. VF1MIN and BK-MIN make use of the

Table 3.4. Format of the file `PROJECT.TRD` . When more than one trajectory is specified, the whole structure is repeated.

Record	Format	Description
1	`1X,A80`	Project header
2	`5H E-W ,A8`	Omnidirectional trapped proton model header
3	`1X,A32`	Header of the internal geomagnetic field model
4	`1X,A32`	Header of the external geomagnetic field model
5	`I3,3X,I3,3X, F8.1,12X,I3`	Numbers of internal and external field models, epoch for internal magnetic field model and number of look directions
6	`F6.1,2F8.1`	Orbit inclination (degrees), perigee height (km) and apogee height (km).
7	`34X,E11.4, 4X, A6`	Total orbit time (hrs) and anisotropy model header
8	`2F10.5`	Polar and azimuthal angle (degrees) of the first look direction
9	`2F10.5, F20.6`	Polar and azimuthal opening angle (degrees) and solid opening angle ($100 = 4\pi$ sr)
10	`I4,16X,2I4`	Number of energies (`NENERP`) in trapped proton spectra, index of the look direction and number of look directions
11	`3E11.4`	Proton energy (MeV), integral ($\mathrm{cm}^{-2}\mathrm{s}^{-1}$) and differential ($\mathrm{cm}^{-2}\mathrm{s}^{-1}\mathrm{keV}^{-1}$) flux
⋮		⋮
10+`NENERP`	`3E11.4`	Proton energy, integral and differential flux
11+`NENERP`		Blank line
12+`NENERP`		Blank line
13+`NENERP`		Blank line
14+`NENERP`		Same as lines 8–(13 + `NENERP`) for the second look direction
⋮		⋮

Table 3.5. Format of the file PROJECT.SPD . When more than one trajectory is specified, the whole structure is repeated.

Record	Format	Description
1	7X,I12,12X, 3I12	Number of look directions (NDIR) and starting date (year, month, day)
2	7X, <NDIR>F12.2	Polar angle for each direction in degrees (DALPH)
3	7X, <NDIR>F12.2	Azimuthal angle for each direction in degrees (DBETA)
4	7X,I12,12X, 3F12.2	Number of energies (NENERP) and location $\bar{p}$ of the satellite (altitude, latitude and longitude)
5	F7.1, <NDIR>E12.4	Energy and conversion factor $W(E, \bar{p}, \zeta, \eta)$ for each direction
⋮		⋮
4+NENERP	F7.1, <NDIR>E12.4	Energy and conversion factor for each direction
5+NENERP		Same as lines 4–(4 + NENERP) for the second location
⋮		⋮
–		Blank line

model AP-8 for solar minimum* while VF1MAX and BK-MAX are defined for solar maximum†. ANISO produces a warning when the omnidirectional model and the anisotropy model are not consistent with each other.

The file PROJECT.TRD produced by ANISO contains the orbit-averaged integral and differential spectra of trapped protons for the different look directions given by (DALPH $= \zeta$, DBETA $= \eta$). The format of the file is described in Table 3.4. For each

*In the TREP namelist, the omnidirectional AP-8 MIN model is correctly selected by the settings: SOLACT = 'MIN', OMNI = 1 and ISPEC = 1. The (B, L) coordinates are then computed with the Jensen and Cain (1962) geomagnetic model.

†In the TREP namelist, the omnidirectional AP-8 MAX model is correctly selected by the settings: SOLACT = 'MAX', OMNI = 1 and ISPEC = 1. The (B, L) coordinates are then computed with the GSFC 12/66 (Cain et al., 1967) geomagnetic model updated to epoch 1970.

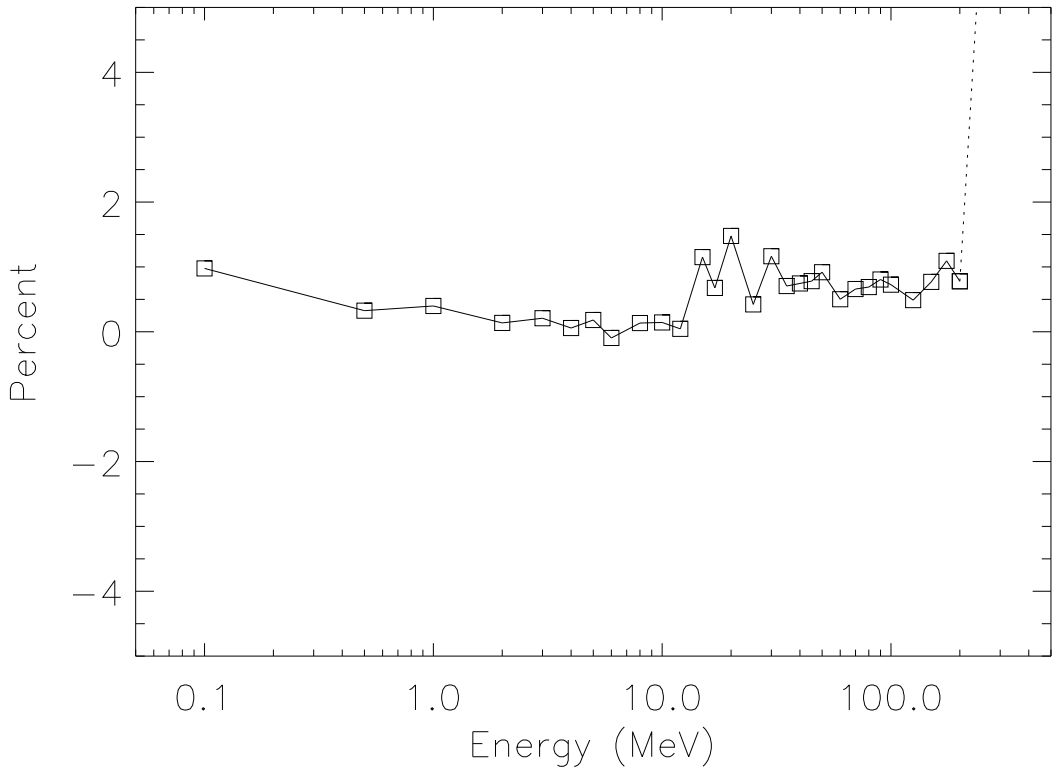

Figure 3.2. Relative difference between the orbit-averaged omnidirectional integral spectrum produced respectively by `ANISO` and by `TREP`. This average is evaluated over fifteen consecutive orbits at 300 km perigee, 2,000 km apogee and 28.5° inclination. The trapped proton models are AP-8 MIN and VF1MIN, respectively for `TREP` and `ANISO`.

look direction, the orbit-averaged trapped proton differential spectra is evaluated as

$$\overline{j}(E,\zeta,\eta) = \frac{\Delta\Omega}{\sum\limits_{\bar{p}} \delta t(\bar{p})} \sum_{\bar{p}} W(E,\bar{p},\zeta,\eta) \left(-\frac{\mathrm{d}J(E,\bar{p})}{\mathrm{d}E}\right) , \tag{3.2}$$

where the summation is taken over each orbital point, δt is the elapsed time between two successive orbit points, $\Delta\Omega$ the opening solid angle (`XOMEGA`), $J(E,\bar{p})$ is the `TREP` omnidirectional integral spectrum and W is the anisotropy correction factor [see Eqs. (2.1) and (1.36)] where the look direction (ζ,η) is related to the correct proton velocity direction (α,ϕ). The orbit-averaged integral spectra are computed as

$$\overline{J}(E,\zeta,\eta) = \int_E^\infty \overline{j}(E',\zeta,\eta)\,\mathrm{d}E' . \tag{3.3}$$

When the namelist parameter `IFULL` is greater than zero, the file `PROJECT.SPD`

is generated. This file contains the angular distribution of the trapped proton fluxes along the orbit. The format of this file is described in Table 3.5.

3.3.1 Program check

To test the ANISO we have calculate the right hand side of the following equality:

$$\overline{J}(E) = \sum_{\zeta,\eta} \overline{J}(E,\zeta,\eta) \tag{3.4}$$

and compared it to the orbit-averaged omnidirectional integral spectrum provided by TREP. In Fig. 3.2, the relative difference (in percentage) between the two spectra is presented as a function of the proton energy. It corresponds to fifteen consecutive orbits at 300 km perigee, 2,000 km apogee and 28.5° inclination. The unidirectional flux is computed over the 180 default look directions. The omnidirectional integral spectrum provided by ANISO is almost identical to the TREP spectrum which is a test of validity of the numerical code. The very small differences are due to

1. the numerical differentiation of the TREP omnidirectional integral spectrum $J(E,\bar{p})$,
2. the approximations in the normalisation of the anisotropy factor $W(E,\bar{p},\zeta,\eta)$,
3. the numerical integration of the orbit-averaged differential spectrum $\overline{j}(E,\zeta,\eta)$,
4. the finite size of the opening solid angle $\Delta\Omega$.

In spite of all these error sources, the differences remain very small. This leads us to conclude that the ANISO program is working well.

3.3.2 ANISOPOS

As a byproduct of ANISO a standalone program called ANISOPOS has also been developed. This program evaluates the trapped proton flux anisotropy at a given single location. ANISOPOS works interactively and is self-explanatory.

The user has to supply a project name, a title, an internal geomagnetic field model [e.g. Jensen & Cain (1962)], the geographical coordinates of a point of observation and he has to select an anisotropy model (e.g. BK-MIN or VF1MIN). The integral flux is generated either by a ASCII input file (PROJECT.TRI) or as a fit to a power law or to an exponential function. Here the user has to input two values of the particle energy corresponding to the range of energy over which the fit is performed and two value of the integral flux. ANISOPOS takes its input interactively from the keyboard. The different commands are given in Table 3.6.

Table 3.6. Interactive menu options of `ANISOPOS`

Code	Action
1	Modify the title
2	Change the geomagnetic field model:
21	– IGRF/DGRF
22	– Jensen and Cain (1962)
23	– GSFC 12/66
3	Modify the epoch of the geomagnetic field model
4	Change the trapped proton anisotropy model:
41	– VF1MIN
42	– VF1MAX
43	– BK-MIN
44	– BKMAX
5	Change the omnidirectional integral flux:
51	– Power law spectrum, defined by two energies and two flux values
52	– Exponentially decreasing spectrum, defined by two energies and two flux values
53	– `PROJECT.TRI`
6	Modify the lower energy of the spectrum
7	Modify the upper energy of the spectrum
8	Specify the geodetic altitude of the point of observation
9	Specify the geodetic latitude of the point of observation
10	Specify the geographic longitude of the point of observation
11	Evaluate the (B, L) coordinates of the point of observation
0	Run the model
-1	Exit and print the results

`ANISOPOS` calculates the unidirectional differential and integral trapped proton fluxes and generates the output files `PROJECT.TRD` and `PROJECT.TRI`.

The file `PROJECT.TRI` contains the omnidirectional fluxes while `PROJECT.TRD` contains the matrix of unidirectional fluxes for a set of look angles.

For non-interactive applications[‡], `ANISOPOS` takes its input from the namelist

[‡]This feature is controlled by the variable `INPLUN` of the common `LUNIOE`. When `INPLUN` is less than zero, the program `ANISOPOS` read a namelist file. In the `UNIRAD` software, the common `LUNIOE`

Table 3.7. ANISOPOS namelist parameters . This namelist is only used for non-interactive applications.

Parameter	Type	Default	Function
TITLE	A*56		Project header
GDALT	R*8	500	Geodetic altitude in km
GDLAT	R*8	-35°	Geodetic latitude in degrees
GDLON	R*8	300°	Geographic longitude in degrees
MODEL	I*4	0	Geomagnetic field model number, from 0 to 2
BLTIME	R*8	1995	Epoch for the geomagnetic field model IGRF
GSFCTIME	R*8	1970	Epoch for the geomagnetic field model GSFC 12/66
JANIS	I*4	1	Anisotropy model number
SPECTRUM	I*4	1	Omnidirectional integral flux number, from 1 to 3. When SPECTRUM = 3, the integral flux is defined by the file PROJECT.TRI.
ENG01	R*8	1	When SPECTRUM is less than 3, energy of the lower limit of the spectrum, in MeV
FJ01	R*8	10^5	When SPECTRUM is less than 3, integral flux at ENG01
ENG10	R*8	10	When SPECTRUM is less than 3, energy of the upper limit of the spectrum, in MeV
FJ10	R*8	10^4	When SPECTRUM is less than 3, integral flux at ENG10

ANISOPOS of the file PROJECT.NML. The parameters of the namelist are listed in Table 3.7.

3.4 Examples

3.4.1 ANISO

In this section, we present the output of a few sample runs of ANISO. The namelist parameters are set to their default value. For all examples, the whole angular distribution of the unidirectional integral (E >20 MeV) flux was calculated and displayed. The orbital parameters RINCL, ORBITS and LONGAPO of the SAPRE namelist are set respectively to 28.5°, 12 and 300°. The orbital parameter HPER is always set

is initialized by the subroutine FILPAR.

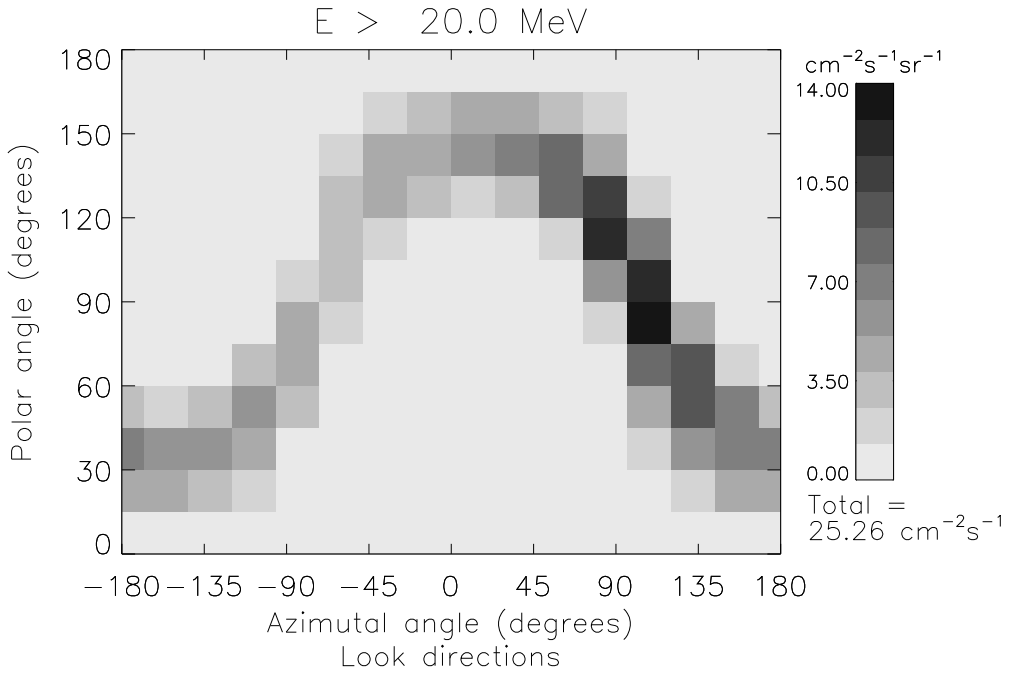

Figure 3.3. Predicted anisotropy of trapped proton integral flux (E >20 MeV) by the VF1MIN anisotropy model. The flux is averaged over twelve consecutive circular orbits (28.5° inclination, 450 km altitude). The polar angle is relative to the zenithal direction and the azimuthal angle relative to geographic North direction in the horizontal plane.

to the same value as `HAPO`, to select a circular orbit. The altitude is set to 450 km (`HPER` = `HAPO` =450 km). In the `TREP` namelist, the `ISPEC` flag is set to 1 to produce the `PROJECT.SPP` output file. The AP-8 MIN model is selected (`SOLACT` = '`MIN`'). The VF1MIN trapped proton anisotropy model is used by setting `JANIS` to 1 in the `ANISO` namelist.

The results displayed in Fig. 3.3 correspond to the case when the satellite orientation is fixed in the horizontal geographic coordinate system (`IATTI` =1 in the `SAPRE` namelist). The orbital parameters are the same as those corresponding to Figs. 2.7 and 2.8 in Sect. 2.4. The unidirectional integral flux varies significantly. It can be seen from Fig. 3.3 that within two zones, looking respectively up to the North and down to the South directions, the flux vanishes. These zones correspond to the loss cone at the position of the satellite. In the directions which are perpendicular to the magnetic field direction, it can be seen that the flux is maximum. Furthermore, the proton flux seen from the West direction is higher than that from the East direction. When the altitude of the satellite is increased, the intensity of all fluxes increases but the anisotropy becomes smoother. However, as stated in Sect. 2.3, the VF1MIN model should not be used to predict trapped proton anisotropy at too high altitude

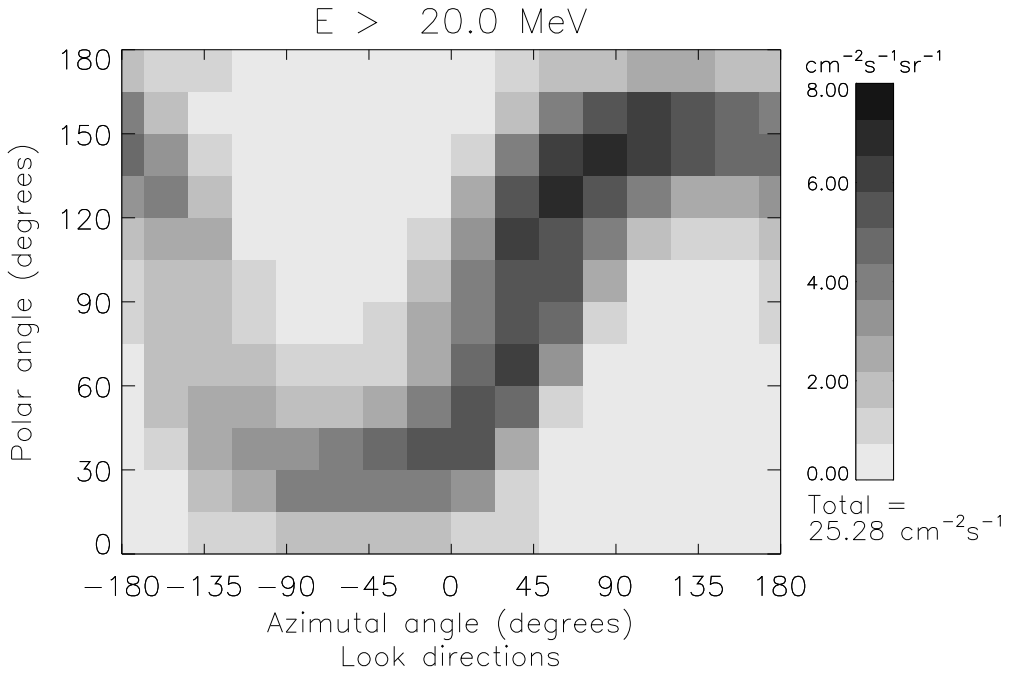

Figure 3.4. Predicted anisotropy of trapped proton integral flux (E >20 MeV) by the VF1MIN anisotropy model. The flux is averaged over twelve consecutive circular orbits (28.5° inclination, 450 km altitude). The polar angle is relative to the geographic North and the azimuthal angle relative to the direction to first point of Aries in the equatorial plane.

(i.e. above 500 km).

The projection of the loss cone in the satellite coordinate system depends on the orbit of the satellite, but also on the orientation or attitude of the satellite along its orbit. In Fig. 3.4, the satellite attitude is fixed relative to the geographical equatorial inertial coordinate system (`IATTI` =3). Surprisely, the angular distribution of the proton fluence is similar to the distribution shown in Fig. 3.3. However, the flux anisotropy is smoother than that in Fig. 3.3. The East-West effect is still observable when the satellite is fixed relative to the geographical equatorial inertial coordinate system.

In the case of Fig. 3.5, the namelist parameter `IATTI` is set to 2. The satellite z-axis points then in direction of the satellite velocity vector. The angular distribution of the proton fluence is then quite different. Due to the orbital characteristics, the trapped proton flux seen on the trailing side is substantially higher than on the leading side. Fig. 3.5 shows that radiation sensitive components should preferably be located on the leading part of the spacecraft: the trailing part of the non-spinning

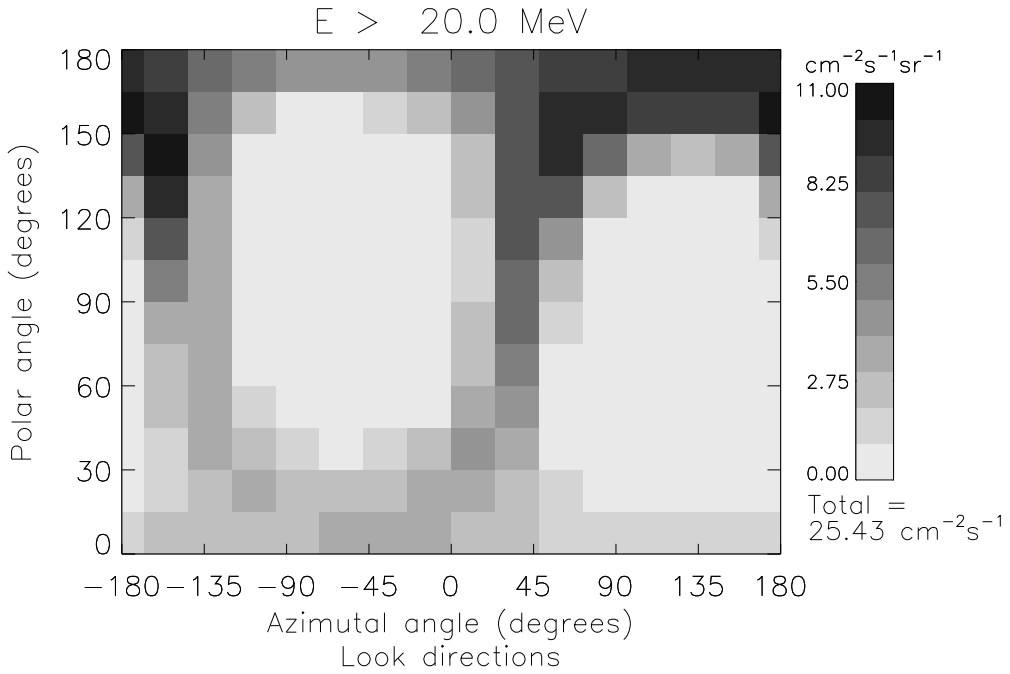

Figure 3.5. Predicted anisotropy of trapped proton integral flux (E >20 MeV) by the VF1MIN anisotropy model. The flux is averaged over twelve consecutive circular orbits (28.5° inclination, 450 km altitude). The polar angle is relative to the direction of the satellite velocity vector. The azimuthal angle is measured in the plane perpendicular to the velocity direction. The zero azimuthal direction is parallel to the orbital plane looking away from the Earth.

spacecraft playing the role of shielding in this case.

Since in Figs. 3.3, 3.4 and 3.5 the orbits are the same, the different orbit-averaged omnidirectional integral fluences given by Eq. (3.4) should be equal. These fluences have be evaluated as a test of the `ANISO` code; they are found to be respectively: 25.26, 25.28 and 25.43 $\mathrm{cm}^{-2}\mathrm{s}^{-1}$. They are clearly a good agreement. The possible origins of the slight differences have been mentioned earlier.

3.4.2 ANISOPOS

A sample run of `ANISOPOS` is presented in Fig. 3.6. It corresponds to the angular distribution of trapped proton differential flux predicted by VF1MIN. The flux is evaluated at the 60°W, 35°S and altitude 450 km. The location and the trapped proton anisotropy model are the same as those used in Fig. 2.2. The omnidirectional

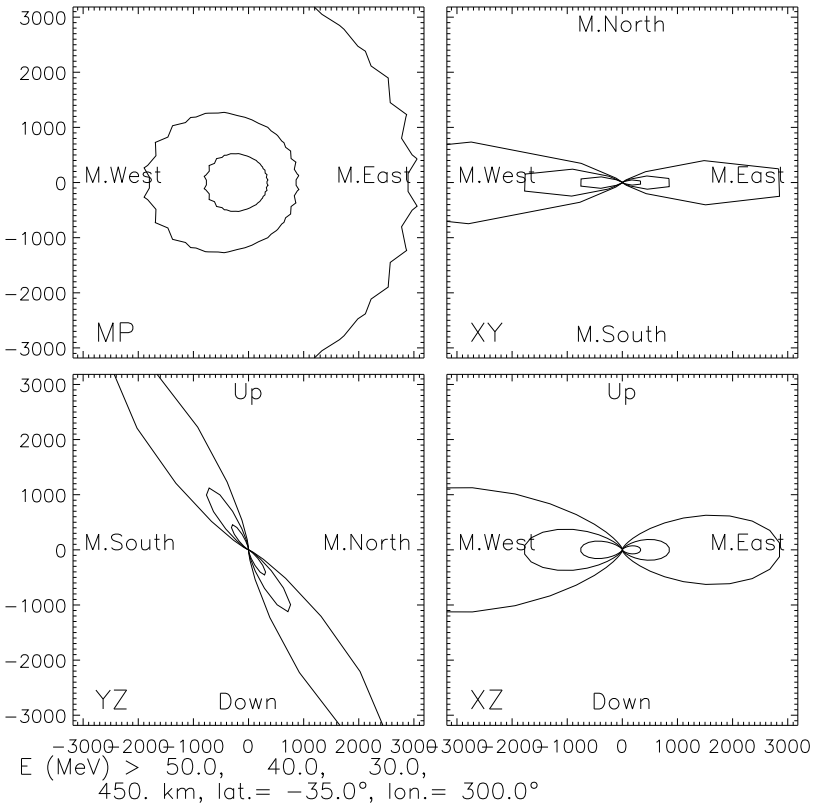

Figure 3.6. Angular distribution of trapped proton integral flux at 60°W, 35°S and altitude 450 km for 30, 40 and 50 MeV proton energies as obtained from the VF1MIN model. The upper left panel corresponds to the local mirror plane. The three other panels correspond to cut view in the planes xy, yz and xz of the satellite coordinate system in the horizontal plane. The z-axis points to the zenithal direction and the x-axis points to the East direction in the horizontal plane.

flux is fixed to

$$J(E) = 10^4 \left(\frac{E}{10\,\mathrm{MeV}}\right)^{-4} \mathrm{cm}^{-2}\mathrm{s}^{-1}\,. \tag{3.5}$$

Each panel of Fig. 3.6 is the polar plot of the angular distribution in a different plane. The radius of each curve is proportional to the directional flux intensity. The different curves correspond respectively to the integral flux for proton energies above E =30, 40 and 50 MeV.

The upper left panel corresponds to the local mirror plane, i.e. the plane which is perpendicular to the magnetic field direction. The horizontal axis corresponds to the intersection between the local mirror plane and the local horizontal plane. This intersection determines the local magnetic East and West directions. The upper left

panel illustrates clearly the East-West effect.

The upper right panel corresponds to a cut view in the local horizontal plane. The horizontal axis is the same as in the upper left panel. The vertical axis lies in the local horizontal plane and is perpendicular to the local magnetic East-West axis: it determines the local magnetic North and South direction. At the point of observation, the loss cone occupies a large fraction of the solid angle.

The lower left and lower right panels correspond to cut views in two vertical planes. At the point of observation, the magnetic field line is parallel to the plane of the lower left panel. The horizontal axis in this panel corresponds to the local magnetic North-South axis. The pitch-angle distribution is nicely illustrated in this panel.

The lower right panel corresponds to the plane perpendicular to the one of the lower left panel. Its horizontal axis corresponds to the magnetic East-West axis. These four panels provide to the user a reliable sketch of the trapped proton anisotropy at the point of observation.

Similar figures can be produced with the BK-MIN and BK-MAX anisotropy model available from the `ANISO` and `ANISOPOS` programs. In Figs. 3.3 to 3.5 we have shown applications of these codes based on the VF1MIN anisotropy model to allow the users compare with results they may have obtained by using the code distributed by MSFC and based on the software developed by Armstrong et al. (1990).

References

Abramowitz, M., Stegun, I.A.: 1964, *Handbook of Mathematical Functions With Formulas, Graphs and Mathematical Tables*, National Bureau of Standards, Applied Mathematics Series **55**

Appleby, M.H., Griffin B.N., Turner E.R., Pogue, W.R., Golightly M.J.: 1992, *Computer Aided Radiation Analysis for Manned Spacecraft*, Proc. 22nd International Conference on Environmental Systems, Seattle, WA, July 13–16

Armstrong, T.W., Chandler, K.C.: 1972, *The High-Energy Transport Code HETC*, Nucl. Sci. Engr. **49**, 110

Armstrong, T.W., Colborn, B.L., Watts, J.W.: 1990, *Characteristics of Trapped Proton Anisotropy at Space Station Freedom Altitudes*, Science Applications International Corporation Report SAIC-90/1474

Armstrong, T.W., Colborn, B.L., Watts, J.W.: 1992a, *Ionizing Radiation Calculations and Comparisons With LDEF Data*, First LDEF Post-Retrieval Symposium, NASA-CP-3134

Armstrong, T.W., Colborn, B.L., Harmon, B.A., Parnell, T.A., Watts, J.W., Jr., Benton, E.V.: 1992b *Comparison of Model Predictions With LDEF Satellite Radiation Measurements*, World Space Congress, 29th Plenary Meeting of COSPAR, Washington D.C., August 29–September 5, Paper F2.7-M.1.06X

Allen, C.W.: 1985, *Astrophysical Quantities*, Third ed., The Athlone Press, London

Badhwar, G.D., Konradi, A.: 1990, *Conversion of Omnidirectional Proton Fluxes Into a Pitch-angle Distribution*, J. Spacecraft and Rockets **27**, 350

Barkas, W.H., Berger M.J.: 1964, *Tables of Energy Losses and Ranges of Heavy Charged Particles*, NAC-NRC Publ. 1133, Nucl. Sci. Ser. Rept. **39**, 103

Blanchard, R.C., Hess, W.N.: 1964, *Solar Cycle Changes in Inner-Zone Protons*, J. Geophys. Res. **69**, 3927–3938

Burrell, M.O.: 1964, *The Calculation of Proton Penetration and Dose Rates*, NASA TM X-53063

Cain, J.C., Hendricks, S.J., Langel, R.A., Hudson, W.V.: 1967, *A Proposed Model for the International Geomagnetic Reference Field-1965*, J. Geomagn. Geoelectr. **19**, 335–355

CIRA: 1965, *1965 Reference Atmosphere*, North-Holland

Colborn, B.L., Watts, J.W., Armstrong, T.W.: 1990, *Data Base Description and Retrieval Program for the Trapped Proton Vector Flux Data Bases VF1MAX and VF1MIN*, Science Applications International Corporation Report SAIC-90/1475

Cornwall, J.M., Allen, R.S., White, R.S.: 1965, *Atmospheric Density Experienced by Radiation Belt Protons*, J. Geophys. Res. **70**, 3099–3111

Evans, H.D.R., Daly E.J.: 1989, *Anisotropies in the Low Altitude Radiation Environment*, Memorandum ESA/ESTEC/WMA

Fano, U.: 1963, *Penetration of Protons, Alpha Particles, and Mesons*, Ann. Rev. Nucl. Sci. **13**, 1–66

Fischer H.M., Auschrat, V.W., Wibberenz, G.: 1977, *Angular Distribution and Energy Spectra of Protons of Energy* $5 < E < 50$ *MeV at the Lower Edge of the Radiation Belt in Equatorial Latitudes*, J. Geophys. Res. **82**, 537–547

Fraser-Smith, A.C.: 1987, *Centered and Eccentric Geomagnetic Dipoles and Their Poles, 1600–1985*, Rev. Geophys. **25**, 1–16

Freden, S.C., White, R.S.: 1960, *Particule Fluxes in the Inner Radiation Belt*, J. Geophys. Res. **65**, 1377–1383

Garcia, H.A., Spjeldvik, W.N.: 1985, *Anisotropy Characteristics of Geomagnetically Trapped Ions*, J. Geophys. Res. **90**, 347–358

Haerendel, G.: 1962, *A Possible Correction to the Spectrum of Geomagnetically Trapped Protons*, J. Geophys. Res. **67**, 1173–1174 and corrigendum, J. Geophys. Res. **67**, 1697

Harwood, J.M., Malin, S.R.C.: 1976, *Present Trends in the Earth's Magnetic Field*, Nature **259**, 469–471

Hassitt, A.: 1965, *Average Effect of the Atmosphere on Trapped Protons*, J. Geophys. Res. **70**, 5385–5394

Heckman, H.H., Brady, V.O.: 1966, *Effective Atmospheric Losses for 125-MeV Protons in South Atlantic Anomaly*, J. Geophys. Res. **71**, 2791–2798

Heckman, H.H., Nakano, G.H.: 1963, *East-West Asymmetry in the Flux of Mirroring Geomagnetically Trapped Protons*, J. Geophys. Res. **68**, 2117–2120

Heckman, H.H., Nakano, G.H.: 1969, *Low-Altitude Trapped Protons during Solar Minimum Period*, 1962-1966, J. Geophys. Res. **74**, 3575–3590

Hedin, A.E.: 1987, *MSIS-86 Thermospheric Model*, J. Geophys. Res. **92**, 4649–4662

Hedin, A.E.: 1991, *Extension of the MSIS Thermosphere Model into the Middle*

and Lower Atmosphere, J. Geophys. Res. **96**, 1159–1172

Heynderickx ,D., Lemaire, J.: 1993, *Improvements to Trapped Radiation Software*, TREND-2 Technical Note 1, Belgian Institute for Space Aeronomy

Heynderickx, D., Lemaire, J.: 1995, *UNIRAD — User Manual*, Belgian Institute for Space Aeronomy

Heynderickx, D., Pierrard, V., Lemaire, J.: 1995, *Atmospheric Cut-off*, TREND-2 Technical Note 2, Belgian Institute for Space Aeronomy

Hess, W.N.: 1968, *The Radiation Belt and Magnetosphere*, Blaisdell Publishing Company, Waltham (Massachusetts)

Jensen, D.C., Cain, J.C.: 1962, *An Interim Geomagnetic Field*, J. Geophys. Res. **67**, 3568–3569

Jentsch, V.: 1984, *The Radial Distribution of Radiation Belts Protons: Approximate Solution of the Steady State Transport Equation at Arbitrary Pitch-angle*, J. Geophys. Res. **89**, 1527–1539

Johnson, F.S.: 1965, *Structure of the Upper Atmosphere*, in Satellite Environment Handbook, second edition, F.S. Johnson, Standford University Press, California, 3–20

Johnson, D.L., Smith, R.E.: 1985, *The MSFC/J70 Orbital Atmosphere Model and the Data Bases for the MSFC Solar Activity Prediction Technique*, NASA TM-86522

Kern, J.W.: 1989, *A Note on Vector Flux Models for Radiation Dose Calculations*, preprint

Knoll, G.F.: 1989, *Radiation Detection and Measurement*, second edition,John Wiley & Sons Inc., New York

Lemaire, J., Daly, E.J., Vette, J.I., McIlwain, C.E., McKenna-Lawlor, S.: 1990, *Secular Variations in the Geomagnetic Field and Calculations of Future Low Altitude Radiation Environments*, Proc. ESA Workshop on Space Environment Analysis, 9–12 Octobre 1990, ESTEC, Noordwijk, The Netherlands, ESA WPP-23

Lemaire, J., Johnstone, A.D., Heynderickx, D., Rodgers, D.J., Szita, S., Pierrard, V.: 1995, *Trapped radiation environment model development TREND-2*, Final Report, contract ESTEC/9828/92/NL/FM, also Aeronomica Acta A **393**

Lenchek, A.M., Singer, S.F.: 1962, *Effects of the Finite Gyroradii of Geomagnetically Trapped Protons*, J. Geophys. Res. **67**, 4073–4075

Liemohn, H.: 1961, *The Lifetime of Radiation Belt Protons with Energies between 1 keV and 1 MeV*, J. Geophys. Res. **66**, 3593–3595

McIlwain, C.E.: 1961, *Coordinates for Mapping the Distribution of Magnetically Trapped Particles*, J. Geophys. Res. **66**, 3681–3691

Newkirk, L.L., Walt, M.: 1964, *Longitudinal Drift Velocity of Geomagnetically Trapped Particles*, J. Geophys. Res. **69**, 1759–1763

Ray, E.C.: 1960, *On the Theory of Protons Trapped in the Earth's Magnetic Field*, J. Geophys. Res. **65**, 1125–1134

Roederer, J.G.: 1970, *Dynamics of Geomagnetically Trapped Radiation*, Springer-Verlag, Berlin

Sawyer, D.M., Vette, J.I.: 1976, *AP-8 Trapped Proton Environment for Solar Maximum and Solar Minimum*, NSSDC/WDC-A-R&S 76-06

Schulz M.: 1995, *Canonical Coordinates in Radiation Belt Modelling*, Workshop on Radiation Belts: Models and Standards, Brussels, October 17–20

Schulz, M., Lanzerotti, L.J.: 1974, *Particle Diffusion in Radiation Belts*, Springer-Verlag, New York

Seltzer, S.M.: 1979, *Electron, Electron-Bremsstrahlung and Proton Depth-Dose Data for Space Shielding Applications*, IEEE Trans. Nucl. Sci. **26**, 4896

Valot, P., Engelmann, J.: 1973, *Pitch-angle Distribution of Geomagnetically Trapped Protons for 1.2< L <2.1*, Space Research XIII, Akademie Verlag, Berlin, 675–681

Vette, J.I.: 1991, *The AE-8 Trapped Electron Model Environment*, NSSDC/WDC-A-R&S 91-24, ch.5

Walt, M.: 1994, *Introduction to Geomagnetically Trapped Radiation*, University Press, Cambridge

Watts, J.W., Parnell, T.A., Heckman, H.H.: 1989, *Approximate Angular Distribution and Spectra for Geomagnetically Trapped Protons in Low-Earth Orbit*, Conf. on High-Energy Radiation in Background Space, A.C. Rester Jr. and J.I. Trombka (Eds.), Santibel Island, FL 1987, Am. Inst. Phys. Conf. Proc., New York, 75–85

Yoshida, S., Ludwig, G.H., Van Allen, J.A.: 1960, *Distribution of Trapped Radiation in the Geomagnetic Field*, J. Geophys. Res. **65**, 807–813

Appendix A

ANISO User Requirements Document

A.1 Introduction

This document contains the User Requirements for the realization of a software. This software will allow users to calculate unidirectional fluences from omnidirectional radiation belt models based on published trapped proton anisotropy models.

This document is a mandatory output of the user requirement phase as described in ESA PSS-05-02 Issue 1 (October 1991) standard for software development.

This work will be accomplished in the framework of the TREND-3 project [contract 10725/94/JG(SG)*]. It is a part of the Work Package 2.2 of the TREND-3 project.

A.1.1 Purpose of the document

The purpose of this document is to state as completely and accurately as possible:

- the kind of users interested in trapped proton anisotropy models;
- the expected features of the software which allow an efficient use of the models;
- the contraints imposed to the software;
- the external input/output of the software needed to interface with other programs.

*ESA Technical Management: E.J. Daly (WMA)

As a result of the user requirement phase, a textual description of these items has been listed. The user requirement phase has been based on the appraisal of BIRA/IASB where experience in Earth's radiation environment has been gained.

A.1.2 Scope of the software

At low altitude, the high-energy trapped proton fluxes are strongly anisotropic and may induce anisotropies in the radiation exposure of a spacecraft with stabilized orientation or attitude. The flux anisotropy results from the interaction of the trapped protons with the Earth's atmosphere and from the finite size of the proton gyroradius which for protons above 10 MeV becomes comparable or larger than the atmospheric scale height. Models of the flux anisotropy are provided to deduce angular dependent proton flux spectra from standard omnidirectional proton flux empirical models which were, until recently, the only radiation environment models available.

The software will implement published anisotropy flux models. This software will be named ANISO and will be a part of the UNIRAD software package which is a suite of programs providing information about the radiation environment along an arbitrary satellite orbit.

This study is useful for scientists and engineers who need empirical models for evaluation of proton fluences for specific space missions within the Earth's radiation environment, especially at low altitude and when the attitude of the spacecraft is not spinning but has a fixed orientation in space.

A.1.3 Definitions, acronyms and abbreviations

This section contains the definitions of terms, acronyms and abbreviations used in the text.

Acronyms and abbreviations

ANSI	American National Standard Institute
AP-8	NASA empirical models for the omnidirectional and unidirectional flux of trapped protons (Sawyer & Vette 1976)
BIRA	Belgisch Instituut voor Ruimte-Aëronomie
DDD	Detailed Design Document
DEC	Digital Equipment Corporation
ESA	European Space Agency
ESTEC	European Space Research and Technology Centre
IASB	Institut d'Aéronomie Spatiale de Belgique
IDL	Interactif Data Language
NASA	National Aeronautics and Space Administration
SRD	Software Requirements Document
TN	Technical Note
TREND	Trapped Radiation ENvironment Development
URD	User Requirements Document
VAX	Virtual Address eXtension
VMS	Virtual Memory System

A.1.4 References

Armstrong, T.W., Colborn, B.L., Watts, J.W.: 1990, *Characteristics of Trapped Proton Anisotropy at Space Station Freedom Altitudes*, Science Applications International Corporation Report SAIC-90/1474

Badhwar, G.D., Konradi, A.: 1990, *Conversion of Omnidirectional Proton Fluxes Into a Pitch-angle Distribution*, J. Spacecraft and Roc. **27**, 350

Heckman, H.H., Nakano, G.H.: 1969, *Low-Altitude Trapped Protons during Solar Minimum Period*, J. Geophys. Res. **74**, 3575–3590

Hess, W.N.: 1968, *The Radiation Belt and Magnetosphere*, Blaisdell Publishing Company, Waltham (Massachusetts)

Lenchek, A.M., Singer, S.F.: 1962, *Effects of Finite Gyroradii of Geomagnetically Trapped Protons*, J. Geophys. Res. **67**, 4073–4075

McIlwain, C.E.: 1961, *Coordinates for Mapping the Distribution of Magnetically Trapped Particles*, J. Geophys. Res. **66**, 3681–3691

Watts, J.W., Parnell, T.A., Heckman, H.H.: 1989, *Approximate Angular Distribution and Spectra for Geomagnetically Trapped Protons in Low-Earth Orbit*,

Conf. on High-Energy Radiation in Background Space, A.C. Rester Jr. and J.I. Trombka (Eds.), Santibel Island, FL 1987, Am. Inst. Phys. Conf. Proc., New York, 75–85

A.1.5 Overview

Section 2 contains the general description of the project. In Section 3 the specific requirements are given.

A.2 General description

A.2.1 Product perspective

The UNIRAD software is a standalone suite of programs. They provide information about the radiation environment in an arbitrary Earth orbit, predicting satellite exposures to particle fluxes, the resulting radiation dosage and the resulting damage-equivalent fluences for solar cell degradation calculations.

The UNIRAD software package includes among others an orbit generator (SAPRE), the computing of the McIlwain's (1961) parameter (BLXTRA), the empirical radiation environment flux models (TREP) and a convertor of energy spectra to radiation dose (SHIELDOSE).

The existing software will be extended to include trapped proton anisotropy models through the implementation of ANISO.

A.2.2 User characteristics

Three categories of potential users can be defined so far:

- scientists engaged in space physics studies;
- aerospace engineers designing space hardware;
- researchers involved in development of models of the near-Earth environment.

A.2.3 General constraints

- The extensions of the software should not modify the use of the UNIRAD software when the ANISO features are bypassed.

- The software programs resulting from the project will be delivered in the form of ANSI Fortran source code conforming to DEC VMS standards.
- The user inputs to the software are done by the way of Fortran namelists.
- The graphical representation of the outputs of the software are realized by the way of IDL routines.

A.2.4 Assumptions and dependencies

The computer resources and personnel to carry out these tasks are available at BIRA-IASB, where experience in software development for the Earth's radiation environment has been gained.

Technical discussions with E.J. Daly will take place on a regular basis at Progress Meetings and during his additional visits to BIRA-IASB. Following these discussions, some of the software requirements which are not mandatory may be reviewed.

A.2.5 Operational environment

Trapped proton anisotropy models depend on different inputs. Some of the inputs may be obtained from the output of existing programs of the UNIRAD software package.

The different inputs are:

- the trajectory of the satellite (it can be computed with the SAPRE program);
- the attitude of the satellite, i.e. its orientation relative to a geodetic coordinate system;
- the (B, L) coordinates of the satellite along its trajectory (it can be calculated by the BLXTRA program);
- the omnidirectional trapped proton flux spectrum at any point along the satellite trajectory (it can be obtained from the TREP program);
- the trapped proton anisotropy model (i.e. a combination of published pitch-angle distributions and East-West asymmetry models).

Typically the output of the trapped proton anisotropy models is an unidirectional integral or differential proton fluences averaged over the satellite trajectory for given directions in the frame of the satellite coordinate system. Such an output may be used to evaluate the radiation dose accumulated inside the satellite during a mission.

A.3 Specific requirements

A.3.1 Essential requirements

1. The UNIRAD package will be able to generate the description of the satellite attitude for a simple case:
   (a) Provide the description of the attitude corresponding to a satellite attitude fixed relative to the Geographic Equatorial Inertial coordinate system.
2. The ANISO program will implement the following models:
   (a) Provide the trapped proton unidirectional flux based on the NASA's omnidirectional flux models AP-8MIN and AP-8 MAX.
   (b) Implementation of the Watts et al. (1989) model. This model takes into account (**1**) Heckman and Nakano's (1969) pitch-angle distribution and (**2**) the finite gyroradius effect described by Lencheck and Singer (1962) for the azimuthal flux distribution.
   (c) Implementation of the empirical pitch-angle distributions proposed by Badhwar and Konradi (1990) and fitted to the unidirectional version of AP-8.
3. The ANISO program will perform the following tasks:
   (a) Compute the orbit-averaged unidirectional integral and differential fluences for the implemented models.
   (b) Perform this calculation for a set of look directions (and viewing angles).
   (c) The look directions or viewing angles of the particle detectors will be fixed in a coordinate system attached to the satellite platform.
4. Graphical representations of the ANISO output has to be provided.

A.3.2 Non-essential requirements

It is desirable to provide a simplified version of the ANISO program to evaluate the anisotropy of trapped proton fluxes at a single and given location in space.

A.3.3 Capability requirements

With the help of the other programs of the UNIRAD package, the ANISO program will generate the geodetic coordinates of a set of points along an orbit specified by the user. It will determine the directional fluence integrated over this orbit.

A.3.4 Constraint requirements

The ANISO program must be implemented into the UNIRAD software package. As a consequence of this implementation:

1. The control parameters must be entered manually by the user in the same way as it is required for the other UNIRAD programs.
2. The input format for the elements defining the satellite trajectory has to be compatible to the SAPRE output format.
3. The input format for the (B, L) coordinates along the satellite trajectory has to be compatible to the BLXTRA output format.
4. The input format for the trapped proton flux spectra along the satellite trajectory has to be compatible to the TREP output format.
5. The output format of the ANISO program has to be (as far as possible) compatible to the SHIELDOSE input format.

Appendix B

ANISO Software Requirements Document

B.1 Introduction

This document contains the Software Requirements for the realization of a software. This software will allow users to calculate unidirectional fluences from omnidirectional radiation belt models based on published trapped proton anisotropy models.

This document is a mandatory output of the software requirement phase as described in ESA PSS-05-02 Issue 1 (October 1991) standard for software development.

This work will be accomplished in the framework of the TREND-3 project [contract 10725/94/JG(SG)*]. It is a part of the Work Package 2.2 of the TREND-3 project.

B.1.1 Purpose of the document

The purpose of this document is to state as completely and accurately as possible:

- the context of the project in relation to past, current and future projects;
- the proposed features of the software and their relevant benefits for the users;
- the description of the logical model;
- the detailed software requirements concerning functionality, performance, interface, operation, resource and documentation of the software.

This document is intended to the developers and the users of the software.

*ESA Technical Management: E.J. Daly (WMA)

B.1.2 Scope of the software

The software will implement existing trapped proton anisotropy flux model. This software will be named ANISO and will be a part of the UNIRAD software package which is a suite of programs providing information about the radiation environment in an arbitrary Earth orbit.

The UNIRAD software package includes among others programs an orbit generator (SAPRE), a program computing the McIlwain's (1961) B and L parameters. (BLXTRA), the empirical radiation environment flux models (TREP), and a program converting the energy spectra to radiation dose (SHIELDOSE).

The ANISO program will transform trapped proton omnidirectional integral fluxes obtained from TREP into unidirectional integral and differential fluxes. These fluxes will be averaged over a user-defined orbit for a user-define attitude of a non-spinning satellite. It will provide trapped proton unidirectional integral and differential fluences.

This software will be useful for scientists and engineers who need empirical models for the evaluation of proton fluences for specific space missions within the Earth's radiation environment at low altitude, especially when the attitude of the spacecraft is non-spinning but has a fixed orientation in space.

B.1.3 Definitions, acronyms and abbreviations

This section contains the definitions of terms, acronyms and abbreviations used in the text.

Acronyms and abbreviations

ANSI	American National Standard Institute
AP-8	NASA empirical models for the omnidirectional and unidirectional flux of trapped protons (Sawyer & Vette 1976)
BIRA	Belgisch Instituut voor Ruimte-Aëronomie
CRRES	Combined Release and Radiation Effects Satellite
DDD	Detailed Design Document
DEC	Digital Equipment Corporation
ESA	European Space Agency
ESTEC	European Space Research and Technology Centre
IASB	Institut d'Aéronomie Spatiale de Belgique
IDL	Interactif Data Language
NASA	National Aeronautics and Space Administration
SAA	South Atlantic Anomaly
SRD	Software Requirements Document
TN	Technical Note
TREND	Trapped Radiation ENvironment Development
URD	User Requirements Document
VAX	Virtual Address eXtension
VMS	Virtual Memory System

B.1.4 References

Armstrong, T.W., Colborn, B.L., Watts, J.W.: 1990, *Characteristics of Trapped Proton Anisotropy at Space Station Freedom Altitudes*, Science Applications International Corporation Report SAIC-90/1474

Badhwar, G.D., Konradi, A.: 1990, *Conversion of Omnidirectional Proton Fluxes Into a Pitch-angle Distribution*, J. Spacecraft and Roc. **27**, 350

Heckman, H.H., Nakano, G.H.: 1969, *Low-Altitude Trapped Protons during Solar Minimum Period*, J. Geophys. Res. **74**, 3575–3590

Hess, W.N.: 1968, *The Radiation Belt and Magnetosphere*, Blaisdell Publishing Company, Waltham (Massachusetts)

Lenchek, A.M., Singer, S.F.: 1962, *Effects of Finite Gyroradii of Geomagnetically Trapped Protons*, J. Geophys. Res. **67**, 4073–4075

McIlwain, C.E.: 1961, *Coordinates for Mapping the Distribution of Magnetically Trapped Particles*, J. Geophys. Res. **66**, 3681–3691

Watts, J.W., Parnell, T.A., Heckman, H.H.: 1989, *Approximate Angular Distribution and Spectra for Geomagnetically Trapped Protons in Low-Earth Orbit*, Conf. on High-Energy Radiation in Background Space, A.C. Rester Jr. and J.I. Trombka (Eds.), Santibel Island, FL 1987, Am. Inst. Phys. Conf. Proc., New York, 75–85

B.1.5 Overview

Section 2 contains the general description of the project. In Section 3 the specific requirements are given.

B.2 General description

B.2.1 Relation to current projects

As part of the TREND-3 study BIRA-IASB is extending and modifying the UNIRAD software package to include trapped proton anisotropy models. This software package is used by ESA for flux, fluence and radiation dose calculations.

B.2.2 Relation to predecessor and successor projects

Experience in software development for modelling of the Earth's radiation environment has been gained at BIRA-IASB during the TREND-1 and TREND-2 studies. Originally the UNIRAD package was integrated in ESABASE but has been transformed into a standalone package.

During TREND-1, the orbit generator (SAPRE) was modified and the computation of the (B, L) (McIlwain, 1961) coordinates was completely reviewed and revised (BLXTRA).

During TREND-2, the BLXTRA program was extended to additional geomagnetic field models and pitch-angle dependent (B, L) coordinates were implemented. The empirical radiation environment flux models (TREP) were extended to accept the directional version of the trapped proton model AP-8 and to include the trapped radiation model CRRESPRO developed by PLGD. The TREP program was modified to guarantee a correct use of the NASA models and to correct for the secular shift of the location of the SAA. IDL routines for graphical representation of the different UNIRAD outputs were delivered.

Future developments may include:

1. implementation of new trapped radiation models in TREP;

2. extension of the trapped proton anisotropy models in ANISO;

3. updating of program convecting energy spectra to radiation dose (SHIELDOSE);

4. realization of a three-dimensional transport code to determine radiation dose distribution inside a spacecraft;

5. restructuring the graphical routines to be more user friendly.

B.2.3 Function and purpose

The extensions of the UNIRAD software package require the modification of the SAPRE program and the development of the ANISO code.

The modification in SAPRE program will require an attitude interface file. For each point along the orbit, the attitude interface file will contain the rotation matrix describing the orientation of the satellite coordinate system with respect to the geocentric spherical coordinate system. This new feature will be controlled by a new parameter in the SAPRE namelist. For each orbit, this parameter will allow to select the orientation of the satellite coordinate system. There are three default cases:

1. The z-axis of the satellite coordinate system points to the zenith. The x-axis and y-axis lie in the horizontal plane and point respectively to the geographic North and West directions.

2. The z-axis of the satellite is parallel to the velocity vector of the satellite. The x-axis lies in the orbital plane, perpendicular to the z-axis and pointing away from the Earth. The y-axis is perpendicular to the orbital plane.

3. The satellite coordinate system is parallel to the geographic equatorial inertial coordinate system.

The realization of the ANISO program will make it possible:

- To compute an orbit-averaged unidirectional proton fluence (integral and differential) based on the omnidirectional flux model AP-8 and on trapped proton flux anisotropy models.

- To use the VF1MIN and VF1MAX models based on the Watts et al. (1989) model and including Heckman and Nakano's (1969) pitch-angle distribution, the East-West effect described by Lencheck and Singer (1962) and the atmospheric scale height proposed by Armstrong et al. (1990).

- To use the BK-MIN and BK-MAX new models based on the Badhwar and Konradi (1990) pitch-angle distribution and the East-West effect described by Lencheck and Singer (1962) with a constant atmospheric scale height.
- To introduce the ANISO input by the way of a namelist file and to provide the results as a formatted text file.

The realization of IDL routines will provide graphical representations of the ANISO outputs which include:

- grayscale plot of the predicted anisotropy of the trapped proton fluence (integral or differential) for a given energy;
- plot to compare the omnidirectional spectrum produced by TREP to the integration over the look directions of the unidirectional spectra produced by TREP;
- surface plot of the predicted angular variation of trapped proton fluence (integral or differential) for a given energy;

A standalone program called ANISOPOS will be derived from the ANISO code. It will allows to evaluate the trapped proton anisotropy at a given location. `ANISOPOS` will work interactively and be self-explanatory.

B.2.4 Environmental considerations

The software will be delivered for VAX and DEC-ALPHA machines which will operate under the VAX/VMS operating system. The IDL software, as well as a text editor have to be implemented.

The software will be used by:

1. scientists engaged in space physics studies;
2. aerospace engineers designing space hardware;
3. researchers involved in development of models of the near-Earth environment.

B.2.5 Relation to other projects

The SAPRE program is a part of the UNIRAD software package and ANISO program will be added to the package. The UNIRAD package is designed as a standalone package but may be implemented in other projects such as

ESABASE This set of programs enables to construct a spacecraft model and analyse it using a framework's applications. It includes among other things, a dedicated editor, a 3D geometry display, a generation of the mass properties and an environmental model for radiation, atmosphere and solar activity.

SPENVIS This system provides access on WWW to most of the space environment models via user-friendly interfaces. It includes among other things, environmental informations on radiation belts, ionospheric plasma, upper-atmospheric oxygen and space debris.

B.2.6 General constraints

– The extensions of the software should not modify the use of the UNIRAD software when the ANISO features are not required.

B.2.7 Model description

This section includes a top-down description of the logical model:

1. Initialize the trapped proton anisotropy model selected by the user.
2. Define the set of look directions and viewing angles in the coordinate system of the satellite.
3. Process each orbit of the satellite:
   (a) Process each orbit element:
      i. Get the position and attitude of the satellite from SAPRE.
      ii. Get the trapped proton omnidirectional differential spectrum:
         A. Get the omnidirectional integral spectrum from TREP
         B. Compute the omnidirectional differential spectrum assuming a power law.
      iii. Evaluate the conversion factor from omnidirectional to unidirectional flux (see below).
      iv. Compute the unidirectional differential flux for the different look directions:
         A. Determine the look directions in the local coordinate system.
         B. Apply the conversion factor to each look direction.
   (b) Compute the unidirectional differential fluence (= orbit-averaged flux) for the different look directions.

(c) Evaluate the unidirectional integral fluence for the different look directions.

(d) Provide the fluences relative to the orbit to the user.

In the ANISO software, the user may select one amongst four trapped proton anisotropy models divided in two categories:

VF1MIN or VF1MAX These models are based on the Watts et al. (1989) proton anisotropy model and on the Armstrong et al. (1990) atmospheric scale height. They make use of the Heckman and Nakano's (1969) pitch-angle distribution model and of the Lencheck and Singer's (1962) theory of the East-West flux asymmetry. VF1MIN and VF1MAX are respectively related to solar minimum and maximum conditions.

BK-MIN or BK-MAX These models combine Badhwar and Konradi's (1990) pitch-angle distribution model with Lencheck and Singer's (1962) theory of the East-West flux asymmetry. BK-MIN and BK-MAX are respectively related to solar minimum and maximum conditions.

The conversion factor from an omnidirectional differential flux to an unidirectional differential flux is specific to each category and has been described in the chapter 1 of the TN 6.

Evaluation for VF1MIN or VF1MAX

1. Compute the pitch-angle distribution:

   (a) Evaluate the magnetic dip angle from the current location and magnetic vector.

   (b) Evaluate the atmospheric scale height from the current altitude.

   (c) Evaluate the normalisation factor.

2. Compute the East-West effect:

   (a) Use the magnetic dip angle and the atmospheric scale height.

Evaluation for BK-MIN or BK-MAX

1. Compute the pitch-angle distribution:

   (a) Retrieve the (B, L) coordinates from TREP.

   (b) Evaluate the parameters of the distribution.

2. Compute the East-West effect:
   (a) Evaluate the magnetic dip angle from the current location and magnetic vector.
   (b) Evaluate the normalisation factor.

B.3 Specific requirements

B.3.1 Functional Requirements

The UNIRAD software consists of a set of standalone programs requiring only one user input file describing the mission characteristics and the models to be used. Running a program entails no more than typing the program name and the project name. The ANISO program will follow these general UNIRAD features.

B.3.2 Performance requirements

No special requirements.

B.3.3 Interface requirements

The user interface shall be kept simple: only one user input file will be required. The software will be operated in command line mode with one single command per program.

B.3.4 Operational requirements

No special requirements.

B.3.5 Resource requirements

The programs included in the UNIRAD software will be developed for VAX/VMS 6.2 or for higher versions. No unusal demands on hardware (e.g. disk space, RAM memory) are made. The graphical routines require an IDL license.

B.3.6 Verification and acceptance test requirements

The UNIRAD software will be installed at ESTEC. A documented sample run will be provided. The system will be tested at ESTEC after installation.

B.3.7 Documentation requirements

The review of the different models underlying the ANISO program and the presentation of a few sample runs will be reported in the TN 6 of the TREND-3 project.

The UNIRAD user manual will be updated with the SAPRE modification and detailed descriptions of the ANISO input and output files.

The architecture design will be added to the UNIRAD ADD.

Detailed descriptions of the newly implemented or modified modules in UNIRAD will be added to the UNIRAD DDD.

B.3.8 Security requirements

This section is not applicable.

B.3.9 Portability Requirements

The software modules for this project shall be conforming to VAX/VMS Fortran. Machine specific code will be avoided so that portability of the code to other operating systems (e.g. DEC-UNIX, UNIX, MS-DOS) is guaranteed.

B.3.10 Quality requirements

The output produced by UNIRAD shall be easy to interpret and to use in other projects.

B.3.11 Reliability requirements

Error trapping shall be implemented for the most commonly occuring error conditions.

B.3.12 Maintainability requirements

The ANISO program will be easily adaptable to include other future trapped proton anisotropy models.

B.3.13 Safety requirements

This section is not applicable.